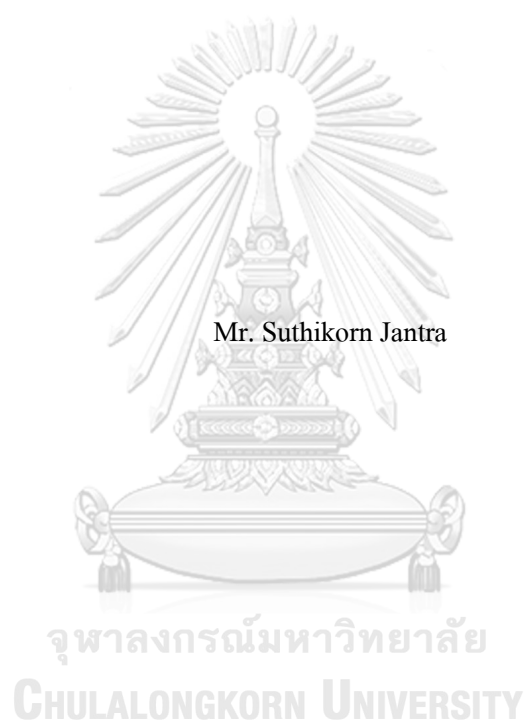


STYRYL-BODIPY FLUORESCENT SENSORS FOR REACTIVE OXYGEN SPECIES  
DETECTION IN CELLS



A Dissertation Submitted in Partial Fulfillment of the Requirements

for the Degree of Doctor of Philosophy in Chemistry

Department of Chemistry

Faculty of Science

Chulalongkorn University

Academic Year 2018

Copyright of Chulalongkorn University

ตัวรับรู้ฟลูออเรสเซนซ์จากสไตริบบอดีไฟสำหรับการตรวจวัดรีแอกทีฟออกซิเจนสปีชีส์ในเซลล์



วิทยานิพนธ์นี้เป็นส่วนหนึ่งของการศึกษาตามหลักสูตรปริญญาวิทยาศาสตรดุษฎีบัณฑิต  
สาขาวิชาเคมี ภาควิชาเคมี  
คณะวิทยาศาสตร์ จุฬาลงกรณ์มหาวิทยาลัย  
ปีการศึกษา 2561  
ลิขสิทธิ์ของจุฬาลงกรณ์มหาวิทยาลัย



สุทธิกร จันทรา : ตัวรับรู้ฟลูออเรสเซนซ์จากสไตริลบอดีปีสำหรับการตรวจวัดรีแอกทีฟ  
 ที่ฟอกซิเจนสปีชีส์ในเซลล์. ( STYRYL-BODIPY FLUORESCENT SENSORS  
 FOR REACTIVE OXYGEN SPECIES DETECTION IN CELLS) อ.ที่ปรึกษาหลัก :  
 รศ. ดร.สัมฤทธิ์ วัชรสินธุ์, อ.ที่ปรึกษาร่วม : ศ. ดร.มงคล สุขวัฒนาสินินท์

ตัวรับรู้เชิงฟลูออเรสเซนซ์เป็นอุปกรณ์ที่มีประโยชน์สำหรับการสังเกตและตรวจวัดรีแอกทีฟที่ฟอกซิเจนสปีชีส์ (ROS) ในเซลล์สิ่งมีชีวิต แม้ว่าตัวรับรู้หลายชนิดจะทำงานได้ดีด้วยการเรืองแสงสีเขียว แต่เพื่อจะเพิ่มประสิทธิภาพการทะลุผ่านเข้าเนื้อเยื่อให้มากที่สุด และลดการรบกวนจากออดีฟลูออเรสเซนซ์ให้เหลือน้อยที่สุด ตัวรับรู้ที่เรืองแสงในช่วงความยาวคลื่นยาวจึงเป็นที่ต้องการ ในงานวิจัยนี้ ตัวรับรู้เชิงฟลูออเรสเซนซ์ชนิดใหม่สามชนิดซึ่งมีพื้นฐานจากบอดีปี ได้แก่ SB1, SB2 และ SB4 ได้ถูกพัฒนาขึ้นสำหรับการตรวจวัด ROS ตัวรับรู้ทั้งสามชนิดมีหมู่สไตริลสองหมู่เชื่อมบนวงไพโรลของบอดีปีเพื่อขยายความยาวคลื่นการเรืองแสงออกไปสู่ช่วงสีแดง (634–662 นาโนเมตร) เราพบว่า SB2 ซึ่งมีทั้งหมู่สไตริลและหมู่ฟินอลในฐานะที่เป็นหน่วยตรวจจับสามารถใช้เป็นตัวตรวจวัด ROS ได้ดีที่สุดในสารละลายที่มีน้ำเป็นองค์ประกอบ ตัวรับรู้ SB2 มีความจำเพาะต่อไฮโดรเจนเปอร์ออกไซด์มากกว่า ROS ชนิดอื่น ๆ โดยแสดงการเปลี่ยนสีจากสีน้ำเงินเป็นสีม่วง และความเข้มแสงฟลูออเรสเซนซ์สัมพันธ์กับความยาวคลื่น 590 นาโนเมตรเพิ่มสูงขึ้น SB2 มีค่าลิมิตการตรวจวัดไฮโดรเจนเปอร์ออกไซด์อยู่ที่ 0.26 ไมโครโมลาร์ ผลึกภัณฑ์ที่เกิดขึ้นจากปฏิกิริยาออกซิเดชันถูกตรวจพบด้วยวิธีแมสสเปกโตรเมตรี ซึ่งช่วยยืนยันกลไกการตรวจวัดของ SB2 ที่มีต่อไฮโดรเจนเปอร์ออกไซด์ SB2 ยังสามารถแพร่ผ่านเข้าไปในเซลล์แมคโครฟาจ RAW264.7 และใช้ตรวจวัดภายในช่วงแสงสีส้ม (570–620 นาโนเมตร) ได้ทั้งไฮโดรเจนเปอร์ออกไซด์ที่เติมจากภายนอกเซลล์และ ROS ที่ผลิตขึ้นภายในเซลล์ซึ่งถูกกระตุ้นด้วยลิโปโพลีแซคคาไรด์ การค้นพบของเราจึงได้นำเสนอตัวรับรู้อีกทางเลือกหนึ่งสำหรับการตรวจวัด ROS ในเซลล์สิ่งมีชีวิต

สาขาวิชา เคมี  
 ปีการศึกษา 2561

ลายมือชื่อนิสิต .....  
 ลายมือชื่อ อ.ที่ปรึกษาหลัก .....  
 ลายมือชื่อ อ.ที่ปรึกษาร่วม .....

## 5672851523 : MAJOR CHEMISTRY

KEYWORD: Sensor, Cell-Imaging, Hypochlorite, BODIPY

Suthikorn Jantra : STYRYL-BODIPY FLUORESCENT SENSORS FOR REACTIVE OXYGEN SPECIES DETECTION IN CELLS. Advisor: Assoc. Prof. SUMRIT WACHARASINDHU, Ph.D. Co-advisor: Prof. MONGKOL SUKWATTANASINITT, Ph.D.

Fluorescent probes are great tools for visualization and imaging of reactive oxygen species (ROS) in living cells. Although several probes perform well with green emission, however, to maximize light penetration for tissue imaging and minimize interference from auto-fluorescence, a probe with longer wavelength is desirable. In this study, three new boron dipyrromethene (BODIPY)-based fluorescent probes SB1, SB2 and SB4 have been developed for detection of ROS. Each probe has two styryl groups anchored to the BODIPY pyrrole rings to extend the emission wavelength into the red region (634–662 nm). Among them, we found that SB2 containing electron-rich p-hydroxyl styryl groups was the best probe for ROS detection. In aqueous media, the probe SB2 demonstrated colorimetric change from blue to purple and gave orange fluorescence turn-on at 590 nm selectively to hypochlorite (NaOCl) over other ROS. SB2 provided the detection limit for NaOCl sensing of 0.26  $\mu\text{M}$ . Several oxidative intermediates were observed from mass spectrometry, suggesting the NaOCl oxidative sensing mechanism of SB2. In RAW264.7 macrophages, SB2 was able to penetrate and detect both exogenous NaOCl and endogenous ROS, induced by lipopolysaccharide (LPS), in the orange field (570–620 nm). Our finding offers long-wavelength probe for ROS detection in live cells.

Field of Study: Chemistry

Student's Signature .....

Academic Year: 2018

Advisor's Signature .....

Co-advisor's Signature .....

## ACKNOWLEDGEMENTS

For the success of my thesis, I would like to thank my thesis advisor Associate Professor Sumrit Wacharasindhu, Ph.D. and co-advisor Professor Mongkol Sukwattanasinitt, Ph.D. for their support and encouragement throughout the course of this research. I also thank exam committees Associate Professor Vudhichai Parasuk, Ph.D., Associate Professor Tanapat Palaga, Ph.D., Associate Professor Kanet Wongravee, Ph.D., Assistant Professor Panuwat Padungros, Ph.D. and Anyanee Kamkaew, Ph.D. for their comments to revise this thesis into complete form.

I would like to express my gratitude to friends and co-workers in MAPS research group, my research won't be achieved without help from them. In group meeting, comments from Associate Professor Paitoon Rashatasakhon, Ph.D., Assistant Professor Anawat Ajavakom, Ph.D. and Assistant Professor Sakulsuk Unarunotai, Ph.D. were also important that I must give my thank to them. For biology part of my research such as cells culture and cytotoxicity test, I would like to thank Patcharavadee Butta from Department of Microbiology and Ponsiree Jithavet and Associate Professor Pornchai Rojsitthisak, Ph.D. from Department of Food and Pharmaceutical Chemistry.

This study is financially supported by the 100th Anniversary Chulalongkorn University Fund for Doctoral Scholarship. This research is also supported by the Thailand Research Fund (RSA6080018 and RTA6180007) and the National Nanotechnology Center, NSTDA, Ministry of Science and Technology, Thailand, through its program of Research Network NANOTEC (RNN). This work is also partially supported by a Grant for International Research Integration: Chula Research Scholar.

Suthikorn Jantra

## TABLE OF CONTENTS

	<b>Page</b>
.....	iii
ABSTRACT (THAI).....	iii
.....	iv
ABSTRACT (ENGLISH).....	iv
ACKNOWLEDGEMENTS.....	v
TABLE OF CONTENTS.....	vi
LIST OF TABLES.....	ix
LIST OF FIGURES.....	x
LIST OF ABBREVIATIONS.....	xiv
CHAPTER I INTRODUCTION.....	1
1.1 Overview.....	1
1.2 Introduction of reactive oxygen species (ROS).....	2
1.2.1 ROS detection methods.....	2
1.2.1.1 <i>Electrochemical analysis</i> .....	2
1.2.1.2 <i>Spin trapping</i> .....	3
1.2.1.3 <i>Chemiluminescence probing</i> .....	3
1.2.1.4 <i>Absorbance probing</i> .....	4
1.2.1.5 <i>Fluorescence probing</i> .....	4
1.3 Introduction of fluorescent sensor.....	4
1.3.1 Basic of fluorophores.....	4
1.3.2 Mechanisms of fluorescent change.....	6

1.3.2.1 Photo-induced electron transfer (PET) .....	6
1.3.2.2 Intramolecular charge transfer (ICT).....	7
1.3.2.3 Excited-state intramolecular proton transfer (ESIPT) .....	8
1.3.2.4 Förster Resonance energy transfer (FRET) .....	8
1.3.3 Modes of fluorescent sensor .....	9
1.3.3.1 Turn-off mode .....	9
1.3.3.2 Turn-on mode.....	9
1.3.3.3 Ratiometric mode.....	9
1.4 Literature review .....	10
1.4.1 Review on Fluorescent probes for ROS detection .....	10
1.4.2 Review on BODIPY-based fluorescent probes for ROS detection.....	11
1.5 Introduction of gold species.....	14
1.5.1 Basic of gold species.....	14
1.5.2 Role of gold in organic reaction.....	14
1.6 Design of our fluorescent probes .....	15
1.7 Objective of this research.....	16
CHAPTER II EXPERIMENTAL .....	17
2.1. Materials.....	17
2.2. Analytical instruments.....	17
2.3. Synthesis of BODIPY probes.....	17
2.3.1. Precursor SB0 .....	17
2.3.2. Probe SB1 .....	19
2.3.3. Probe SB2 .....	19
2.3.4. Probe SB4 .....	20



2.4. Preparation of ROS and metal ions .....	21
2.5. Cell culture .....	21
2.6. Cytotoxicity of SB2 on RAW264.7 cells .....	21
2.7. Cells imaging.....	22
2.7.1. SB2-stained cells.....	22
2.7.2. Exogenous NaOCl.....	22
2.7.3. Endogenous ROS .....	22
2.7.4. Samples preparation for confocal laser microscopy .....	22
Chapter III RESULTS AND DISCUSSION .....	23
3.1 Synthesis of probes SB1–4.....	23
3.2 Photophysical properties of SB0, SB1, SB2 and SB4.....	25
3.3 Response of SB2 and SB4 toward Au <sup>3+</sup> .....	26
3.4 Response of SB2 toward ROS in the absence and presence of Au <sup>3+</sup> .....	30
3.5 Optimization condition for SB2 toward NaOCl sensing.....	34
3.6 Sensitivity of SB2 toward NaOCl.....	36
3.7 Proposed reaction mechanism between SB2 and NaOCl.....	39
3.8 Cell-imaging application.....	40
CHAPTER IV CONCLUSIONS .....	44
REFERENCES .....	46
APPENDIX.....	50
VITA .....	55

## LIST OF TABLES

	<b>Page</b>
Table 3.1 Photophysical properties of SB0, SB1, SB2 and SB4 in MeOH.....	26



## LIST OF FIGURES

	<b>Page</b>
Figure 1.1: Generations of reactive oxygen species in biological system [12].....	2
Figure 1.2: Relation between hydroxyl radical and electrochemical cell.....	3
Figure 1.3: Reaction between nitron compound and hydroxyl radical.....	3
Figure 1.4: Reaction between $\text{Ru}(\text{bpy})_3^{3+}$ and hydroxyl radical.....	3
Figure 1.5: reaction between NBT and superoxide anion.....	4
Figure 1.6: Jablonski diagram.....	5
Figure 1.7: Common fluorophores.....	6
Figure 1.8: Response of the probe GSB toward cyanide ion.....	6
Figure 1.9: Energy diagram of fluorescent probe a) with PET and b) without PET [27].....	7
Figure 1.10: Energy diagram of fluorescent probe with ICT process [26].....	7
Figure 1.11: Energy diagram of fluorescent probe with ESIPT process [28].....	8
Figure 1.12: Energy diagram of fluorescent probe with FRET process [29].....	8
Figure 1.13: Modes of fluorescent sensor.....	9
Figure 1.14: Reaction of probe 1 toward $\text{H}_2\text{O}_2$ .....	10
Figure 1.15: Reaction of HRS1 with $\text{OCl}^-$ .....	11
Figure 1.16: Response of DCHP toward $\text{H}_2\text{O}_2$ .....	11
Figure 1.17: Ratiometric sensing of probe 7 toward ROS.....	12
Figure 1.18: Response of probe OHP toward $\bullet\text{OH}$ .....	12
Figure 1.19: Response of probe OX-PPA-BODIPY toward $\text{ClO}^-$ .....	13
Figure 1.20: Response of BODIPY-Se toward $\text{H}_2\text{O}_2$ .....	14
Figure 1.21: Gold-catalyzed organic transformations.....	15

Figure 1.22: Design of styryl-BODIPY probes and hypothesis on gold-catalyzed oxidation.....	16
Figure 1.23: Chemical structure of the probes SB1–4.....	16
Figure 2.24: preparation of SB0.....	18
Figure 2.25: Preparation of SB1 .....	19
Figure 2.26: Preparation of SB2 .....	19
Figure 2.27: Preparation of SB4 .....	20
Figure 3.28: Chemical structure of probes SB1–4.....	23
Figure 3.29: Preparation of probes SB1–4.....	24
Figure 3.30: <sup>1</sup> H-NMR spectra of SB0, SB1, SB2 and SB4.....	25
Figure 3.31: Absorption (bold line) and emission (dash line) spectra of SB0, SB1 and SB2, inset: Images of SB0, SB1, SB2 and SB4 in MeOH under room light and black light. ....	26
Figure 3.32: Gold-catalyzed organic transformations.....	27
Figure 3.33: Absorption spectra (a,c), emission spectra (b,d; $\lambda_{\text{Ex}} = 540 \text{ nm}$ ) of 5 $\mu\text{M}$ SB2 (a,b) and 4 $\mu\text{M}$ SB4 (c,d) in the presence of 10 equivalents metal ions including $\text{Li}^+$ , $\text{Na}^+$ , $\text{K}^+$ , $\text{Mg}^{2+}$ , $\text{Ca}^{2+}$ , $\text{Ba}^{2+}$ , $\text{Al}^{3+}$ , $\text{Cr}^{3+}$ , $\text{Fe}^{2+}$ , $\text{Fe}^{3+}$ , $\text{Co}^{2+}$ , $\text{Ni}^{2+}$ , $\text{Cu}^{2+}$ , $\text{Zn}^{2+}$ , $\text{Pb}^{2+}$ , $\text{Hg}^{2+}$ , $\text{Cd}^{2+}$ , $\text{Ag}^+$ and $\text{Au}^{3+}$ . All samples were measured after 1 hour of mixing in solution (4/1 v/v of MeOH/HEPES buffer pH 7). ....	28
Figure 3.34: Fluorescence enhancement ratio ( $\lambda_{\text{Ex}} = 540 \text{ nm}$ ) of 5 $\mu\text{M}$ SB2 (a) and 4 $\mu\text{M}$ SB4 (b) in the presence of 10 equivalents metal ions including $\text{Li}^+$ , $\text{Na}^+$ , $\text{K}^+$ , $\text{Mg}^{2+}$ , $\text{Ca}^{2+}$ , $\text{Ba}^{2+}$ , $\text{Al}^{3+}$ , $\text{Cr}^{3+}$ , $\text{Fe}^{2+}$ , $\text{Fe}^{3+}$ , $\text{Co}^{2+}$ , $\text{Ni}^{2+}$ , $\text{Cu}^{2+}$ , $\text{Zn}^{2+}$ , $\text{Pb}^{2+}$ , $\text{Hg}^{2+}$ , $\text{Cd}^{2+}$ , $\text{Ag}^+$ and $\text{Au}^{3+}$ . Inset: image of solutions under room light and black light. All samples were measured after 1 hour of mixing in solution (4/1 v/v of MeOH/HEPES buffer pH 7). ....	29
Figure 3.35: Confocal microscopic images ( $\lambda_{\text{Ex}}\lambda_{\text{Em}} = 561/595 \text{ nm}$ ) of RAW264.7 macrophages before and after incubation with SB2 (5 $\mu\text{M}$ ), and then treated the stained cells with $\text{Au}^{3+}$ (5 $\mu\text{M}$ ). .....	30

- Figure 3.36: Enhancement ratio at 590 nm ( $\lambda_{\text{ex}} = 540$  nm) of SB2 (5  $\mu\text{M}$ ) toward various ROS (50  $\mu\text{M}$ ) with or without  $\text{Au}^{3+}$  (5  $\mu\text{M}$ ). All samples were measured after 30 minutes of mixing in solution (4/1 v/v of MeOH/HEPES buffer pH 7). .....31
- Figure 3.37: Emission spectra ( $\lambda_{\text{ex}} = 540$  nm) of 5  $\mu\text{M}$  SB2 toward various ROS (2.5 equivalents), inset: enhancement ratio and Images of each solution. All samples were measured after 30 minutes of mixing in solution (3/2 v/v of MeOH/PBS (10 mM) pH 7.4). .....32
- Figure 3.38: Absorption (a–c) and emission (e–g; excitation wavelength at 480 nm for SB0 and 540 nm for SB1 and SB2) spectra of SB0, SB1 and SB2 (5  $\mu\text{M}$ ) in the absence (bold line) and presence (dash line) of 1 equivalent NaOCl. Absorbance (d) and fluorescence (h) enhancement ratio. All samples were measured after 30 minutes of mixing in 4/1 (v/v) of MeOH/PBS (10 mM) pH 7.4.....33
- Figure 3.39: Emission spectra ( $\lambda_{\text{ex}} = 540$  nm) of 5  $\mu\text{M}$  SB2 in various organic solvents after addition of 1 equivalent NaOCl for 30 minutes. Inset: Fluorescence enhancement ratios at 590 nm. ....34
- Figure 3.40: a) Fluorescence enhancement ratio of SB2 in 0–100% MeOH before and after addition of 2.5 equivalents NaOCl for 30 minutes. Inset: Images of the solutions under black light in the absence and presence of NaOCl. b) Fluorescent intensity of SB2 in 3/2 (v/v) of MeOH/PBS (10 mM) pH 4–10 in the absence and presence of 2.5 equivalents NaOCl. c) Fluorescence enhancement ratio of SB2 in (3/2 v/v) of MeOH/PBS (10 mM) pH 7.4 in the presence of 1 or 2.5 equivalents NaOCl at various time. All samples used 5  $\mu\text{M}$  SB2 (excitation wavelength at 540 nm and emission wavelength at 590 nm). .....36
- Figure 3.41: Absorption spectra (a), emission spectra under excitation at 540 (b) and 480 (c) nm and sensitivity plot (d) of SB2 (5  $\mu\text{M}$ ) toward NaOCl (0–10 equivalents), inset: images of solutions under room light (a) and black light (d). All samples were measured after 30 minutes of mixing in 3/2 (v/v) of MeOH/PBS (10 mM) pH 7.4. ....38
- Figure 3.42: Emission spectra of SB2 (5  $\mu\text{M}$ ) toward NaOCl (0–5  $\mu\text{M}$ ), inset: linear relation of fluorescence intensity vs NaOCl concentration. All samples were measured after 30 minutes of mixing in 3/2 (v/v) of MeOH/PBS (10 mM) pH 7.4. ....39

Figure 3.43: a) MALDI-TOF mass spectrum from mixture of SB2 (5 $\mu\text{M}$ ) and NaOCl (5 equivalents) in MeOH and b) proposed reaction mechanism between SB2 and NaOCl.....	40
Figure 3.44: MTT assay against RAW264.7 cells in the absence and presence of LPS (1 $\mu\text{g}/\text{mL}$ ) before and after treatment with of SB2 (1 and 10 $\mu\text{M}$ ).....	41
Figure 3.45: Confocal microscopic images of murine macrophages RAW264.7 before (a) and after (b) incubation with SB2 (1 $\mu\text{M}$ ) followed by treatment with NaOCl at 1 (c), 2.5 (d) or 10 $\mu\text{M}$ (e). .....	42
Figure 3.46: Confocal microscopic images of murine macrophages RAW264.7 in the absence (a) and presence of LPS at 0.1 (b), 1 (c), 2.5 (d) and 10 $\mu\text{g}/\text{mL}$ (e) after incubation with SB2 (1 $\mu\text{M}$ ). .....	43
Figure 3.47: Mean grey values (subtracted by blank) of fluorescent signal from SB2 in RAW264.7 cells stimulated with LPS at 0–10 $\mu\text{g}/\text{mL}$ . .....	43
Figure A.48: $^1\text{H}$ -NMR spectrum of SB0 in $\text{CDCl}_3$ .....	50
Figure A.49: $^{13}\text{C}$ -NMR spectrum of SB0 in $\text{CDCl}_3$ .....	50
Figure A.50: ESI-HRMS spectrum of SB0.....	50
Figure A.51: $^1\text{H}$ -NMR spectrum of SB1 in $\text{CDCl}_3$ .....	51
Figure A.52: $^{13}\text{C}$ -NMR spectrum of SB1 in $\text{CDCl}_3$ .....	51
Figure A.53: ESI-HRMS spectrum of SB1.....	51
Figure A.54: $^1\text{H}$ -NMR spectrum of SB2 in acetone- $\text{D}_6$ .....	52
Figure A.55: $^{13}\text{C}$ -NMR spectrum of SB2 in $\text{DMSO}-\text{D}_6$ .....	52
Figure A.56: ESI-HRMS spectrum of SB2.....	52
Figure A.57: $^1\text{H}$ -NMR spectrum of SB4 in $\text{DMSO}-\text{D}_6$ .....	53
Figure A.58: $^{13}\text{C}$ -NMR spectrum of SB4 in $\text{DMSO}-\text{D}_6$ .....	53
Figure A.59: ESI-HRMS spectrum of SB4.....	53

## LIST OF ABBREVIATIONS

Ab	Absorption
BODIPY	Boron-dipyrrromethene
CCA	2-Cyano-4-hydroxycinnamic acid
DCM	Dichloromethane
DDQ	2,3-Dichloro-5,6-dicyano-1,4-benzoquinone
DIPEA	<i>N,N</i> -Diisopropylethylamine
DMEM	Dulbecco's Modified Eagle Medium
DMSO	Dimethyl sulfoxide
DNA	Deoxyribonucleic acid
Em	Emission
EPR	Electron paramagnetic resonance
ESIPT	Excited-state intramolecular proton transfer
ESI	Electrospray ionization
ESR	Electron spin resonance
Ex	Excitation
FBS	Fetal Bovine Serum
FRET	Forster resonance energy transfer
HOMO	Highest occupied molecular orbital
HRMS	High-resolution mass spectrometry
ICT	Intramolecular charge transfer
IR	Infrared
LPS	Lipopolysaccharide
LUMO	Lowest unoccupied molecular orbital
M	Molar
mg	milligram
mL	millilitre
mmol	millimole
MTT	3-(4,5-dimethylthiazol-2-yl)-2,5-diphenyltetrazolium bromide

nm	nanometer
NMR	Nuclear magnetic resonance
PBS	Phosphate buffer saline
PET	Photo-induced electron transfer
ppm	parts per million
ROS	Reactive oxygen species
TLC	Thin-layer chromatography
UV-vis	Ultraviolet-visible
vs	versus





## CHAPTER I INTRODUCTION

### 1.1 Overview

Reactive oxygen species (ROS) are ions or molecules containing reactive oxygen atom such as hydroxyl radical, superoxide anion, hydrogen peroxide, singlet oxygen and hypochlorite. They are important signaling molecules for various metabolism in biological system. Their concentration involves the state of health and disease [1]. However, overproduction of ROS from oxidative stress in biological cells causes the overoxidation of biomolecules, such as enzymes, cellular membranes and DNA, leading to permanent cellular damage [2] and various diseases including osteoarthritis [3], atherosclerosis [4], neurodegeneration [5] and nephropathy [6]. Therefore, the medical and biological researches involved with the functions of ROS require biocompatible and sensitive tool for imaging and mechanistic study of ROS generation in live cells, which lead to better understanding of biological processes and clinical diagnostics.

Among various methods for determination of ROS [7, 8], fluorescent sensor is a suitable tool for monitoring and imaging the ROS in biological system [9]. Many fluorescent probes for selective detection of ROS in recent years have been reported [10-12], utilizing pyrene [13], coumarin [14], fluorescein [15], rhodamine [16], naphthalimide [17], and boron-dipyrromethene (BODIPY) as a fluorophore. Among them, BODIPY offers many outstanding advantages including excellent photostability, flexible modification, high molar absorptivity and biocompatibility [18] which provides its popularity in live cell imaging. However, most BODIPY-based fluorescent probes are effective in the green-emissive region (shorter than 530 nm) which is relatively short wavelength and requires high excitation energy. The short-wavelength probes usually suffer from low cellular penetration, biomolecular autofluorescence and are damaging to living cells. Some of them gives turn-off fluorescence signal which can easily provide false positive result. Based on mentioned drawbacks, we therefore want to prepare orange-red emissive BODIPY probe for ROS detection. Based on the literature, gold species has been known as a catalyst for oxidation of styrene into epoxide, aldehyde, and ketone compounds in the presence of ROS [19]. With this knowledge, we design the new fluorescent probe based on BODIPY conjugating with styrene to extend  $\pi$ -conjugation in combination with gold. This system should allow us to create near-IR probe with high sensitivity toward ROS.

## 1.2 Introduction of reactive oxygen species (ROS)

Reactive oxygen species (ROS) are ions or molecules containing oxygen atom such as oxygen gas ( $O_2$ ), singlet oxygen ( $^1O_2$ ), superoxide anion ( $O_2^-$ ), hydrogen peroxide ( $H_2O_2$ ), alkyl hydroperoxide (ROOH), hydroxyl radical ( $\cdot OH$ ) and hypochlorite anion ( $ClO^-$ ) (Figure 1.1). Depend on ROS level in the system, they can act as oxidizing agents for many organic reactions and biological processes including normal cell growth, induction and maintenance of the metabolism, apoptosis and even genomic mutation which leads to tumor [1]. Therefore, ROS concentration is an important key for controlling the state of health and disease.

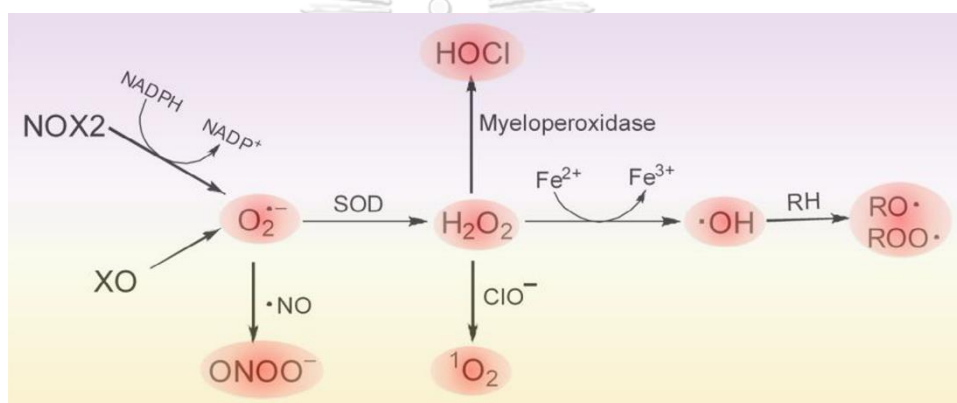


**Figure 1.1:** Generations of reactive oxygen species in biological system [12]

### 1.2.1 ROS detection methods

There are several methods for determination of ROS including electrochemical analysis, spin-trapping, chemiluminescence probing, absorbance probing and fluorescence probing [8].

#### 1.2.1.1 Electrochemical analysis

Electrochemical analysis is an indirect method using correlation between amount of ROS in the electrolytic cell and amount of electric signal generated. Gualandi and Tonelli [20] used a polyphenol-coated electrode together with the redox pair  $Ru(NH_3)_6^{3+}/Ru(NH_3)_6^{2+}$ . Hydroxyl radical could degrade the film, resulting in uncovered area on the electrode and completion of electrical circuit (Figure 1.2).

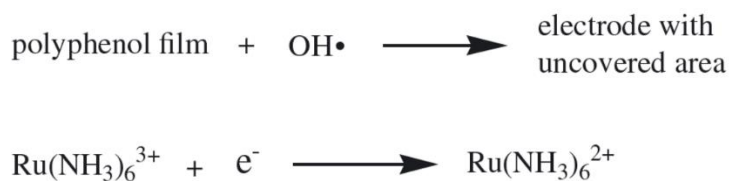


**Figure 1.2:** Relation between hydroxyl radical and electrochemical cell

### 1.2.1.2 Spin trapping

This method relies on reaction between nitron or nitroso compound and radical ROS such as  $^1\text{O}_2$ ,  $\bullet\text{OH}$  and peroxy radical (Figure 1.3). Amount of nitroxide adduct, which correlate to amount of ROS, can be determined by electron spin/paramagnetic resonance spectroscopy (ESR/EPR) [21].

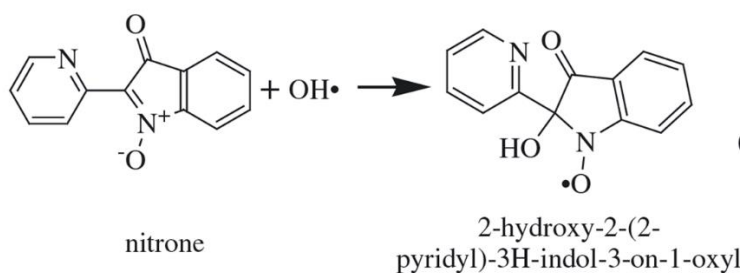


**Figure 1.3:** Reaction between nitron compound and hydroxyl radical

### 1.2.1.3 Chemiluminescence probing

This method relies on reaction between chemiluminogenic compound and ROS, resulting in production of an excitation that can be measured by luminometer. Nobushi and Uchikura [22] used  $\text{Ru}(\text{bpy})_3^{3+}$  as a probe for detection of  $\bullet\text{OH}$  (Figure 1.4).

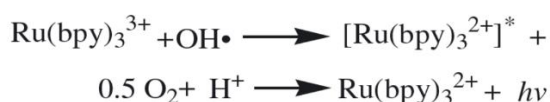


**Figure 1.4:** Reaction between  $\text{Ru}(\text{bpy})_3^{3+}$  and hydroxyl radical

#### 1.2.1.4 Absorbance probing

This method relies on the reduction of probe absorbance or enhancement of product absorbance upon the addition of ROS. The absorbance can be measured by UV-vis spectrophotometer. Xu and co-worker [23] used nitroblue tetrazolium (NBT) as a probe for detection of superoxide ion. NBT could undergo redox reaction with superoxide anion, resulting in absorbance reduction at 259 nm (Figure 1.5).

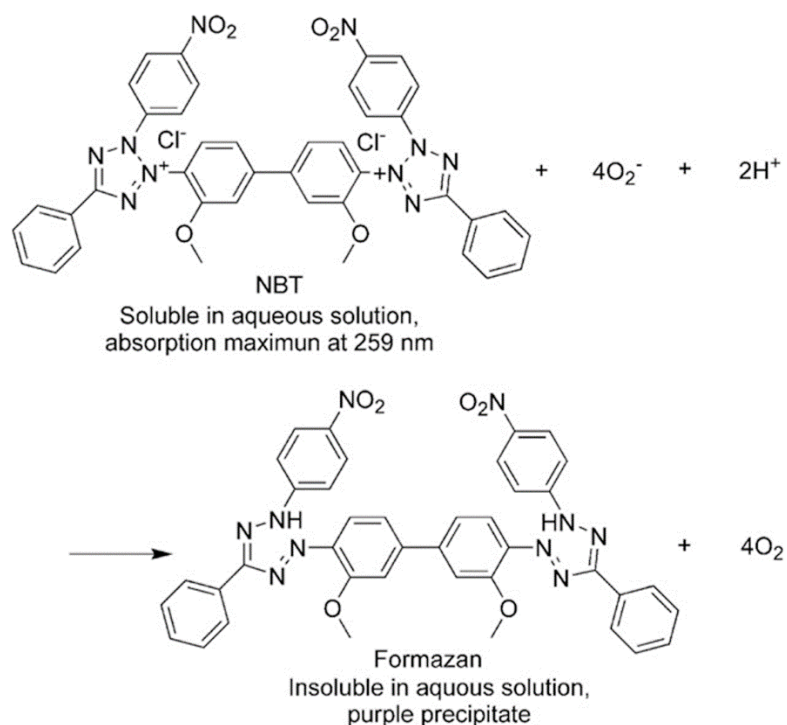


**Figure 1.5:** reaction between NBT and superoxide anion

#### 1.2.1.5 Fluorescence probing

This method relies on the reaction between fluorescent probe and ROS, resulting in change of fluorescent signal. The detail of this method will be described thoroughly in section 1.3.

### 1.3 Introduction of fluorescent sensor

#### 1.3.1 Basic of fluorophores

Fluorophore or chromophore is chemical compound which can absorb and re-emit light in the visible region (380–780 nm). Emission wavelength is usually longer than absorption wavelength, which can be explained by Jablonski diagram (Figure 1.6) [24]. Initially, energy of

fluorophore is at ground state  $S_0$ . Upon excitation energy, fluorophore is induced into excited state  $S_1$  with high vibrational energy. Then it releases non-radiative energy in the form of heat or vibration to be at most stable excited state. Finally, fluorophore drops back to  $S_0$  and release emission energy as fluorescence light. The wavelength and intensity of this fluorescence light can be measured by fluorescence spectrophotometer. This property can be applied as a signaling unit for fluorescence sensor method.

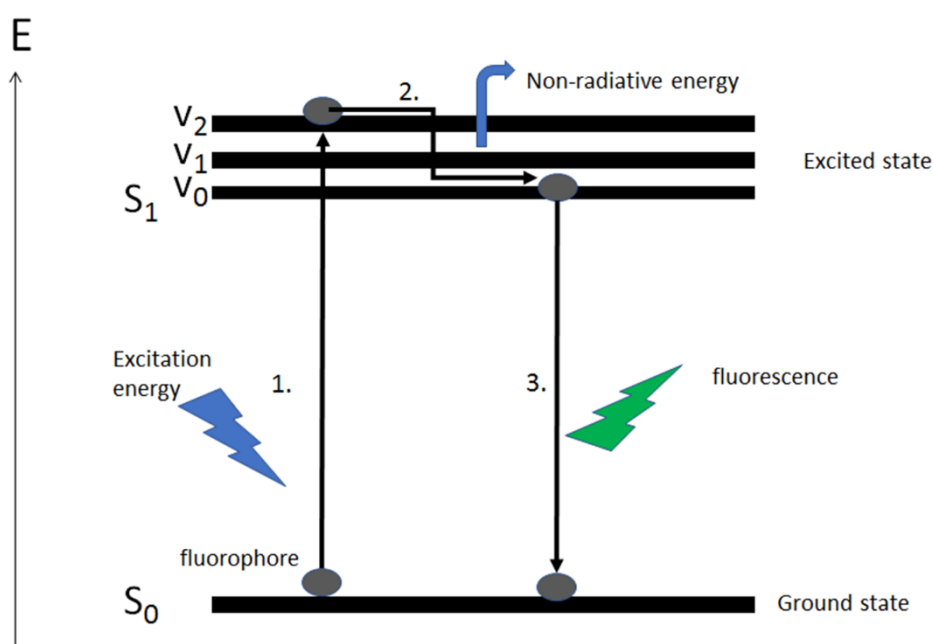
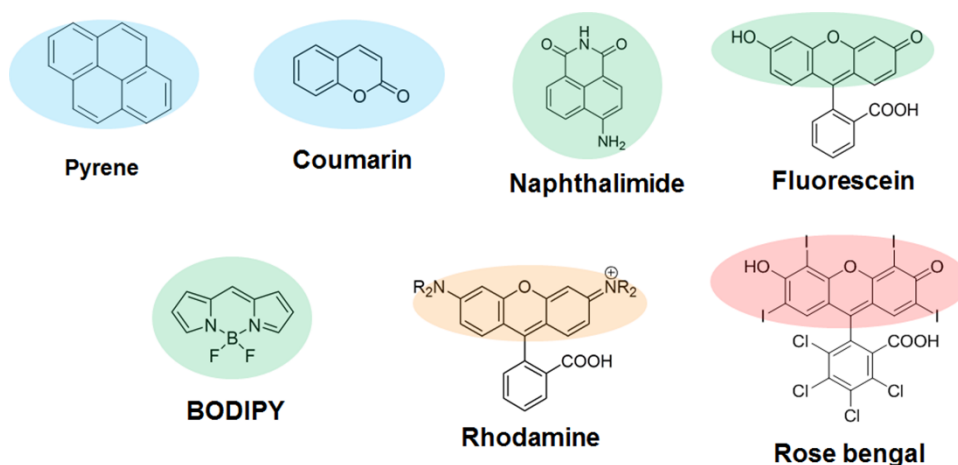
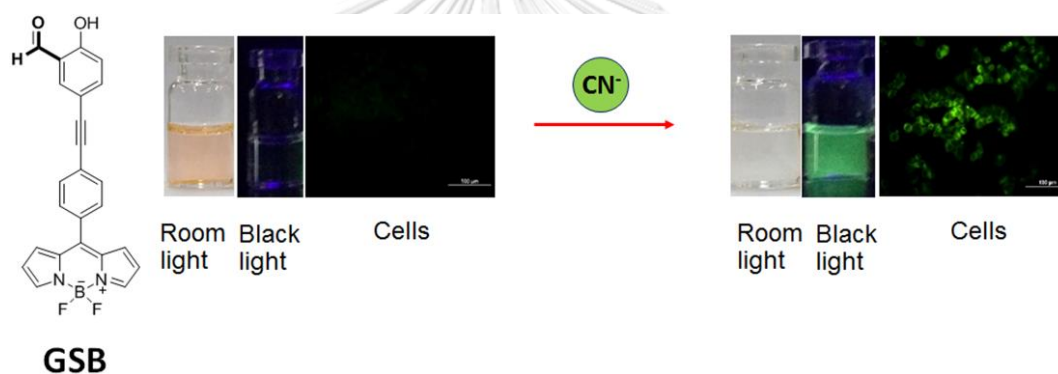


Figure 1.6: Jablonski diagram

There are many fluorophores that have been used as commercial dyes with various fluorescent color available (Figure 1.7). Their structures can also be modified to get desired photophysical properties, including absorption wavelength ( $\lambda_{Ab}$ ), molar absorptivity ( $\epsilon$ ), emission wavelength ( $\lambda_{Em}$ ) and quantum yield ( $\theta_f$ ). Among them, boron-dipyrromethene (BODIPY) is in our interest due to its unique properties such as high photostability, high quantum yield and narrow emission bandwidth. It is also easy to modify BODIPY structure to contain functional group which acts as receptor for binding with analyte, resulting in fluorescent change. For example, our group have developed a BODIPY-based fluorescent probe **GSB** containing salicylaldehyde moiety [25]. The probe could response to cyanide ion selectively in both solution and live cell, resulting in green-fluorescent enhancement (Figure 1.8).



**Figure 1.7:** Common fluorophores



**Figure 1.8:** Response of the probe **GSB** toward cyanide ion

### 1.3.2 Mechanisms of fluorescent change

When a fluorophore is applied as a component of fluorescent probe, receptor is another component in the same molecule which can affect the fluorescence upon interaction with analyte. The most widely utilized fluorescent signaling mechanisms are photo-induced electron transfer (PET), Intramolecular charge transfer (ICT), Excited-state intramolecular proton transfer (ESIPT) and Förster Resonance energy transfer (FRET) processes [26].

#### 1.3.2.1 Photo-induced electron transfer (PET)

Normally, upon excitation, an electron of fluorophore at HOMO (highest occupied molecular orbital) level will be excited into LUMO (lowest unoccupied molecular orbital) level.

Drop back of the electron to the HOMO corresponds to the release of fluorescence. Photo-induced electron transfer (PET) is a process in which fluorophore and receptor are separated by aliphatic spacer and receptor has HOMO energy level in between HOMO and LUMO of excited fluorophore. HOMO of excited fluorophore will be occupied by an electron transferred from the receptor, leading to inability of electron in LUMO to drop back and resulting in fluorescent quenching (Figure 1.9a). However, interaction of receptor and suitable analyte will inhibit PET process and recover the fluorescent signal (Figure 1.9b).

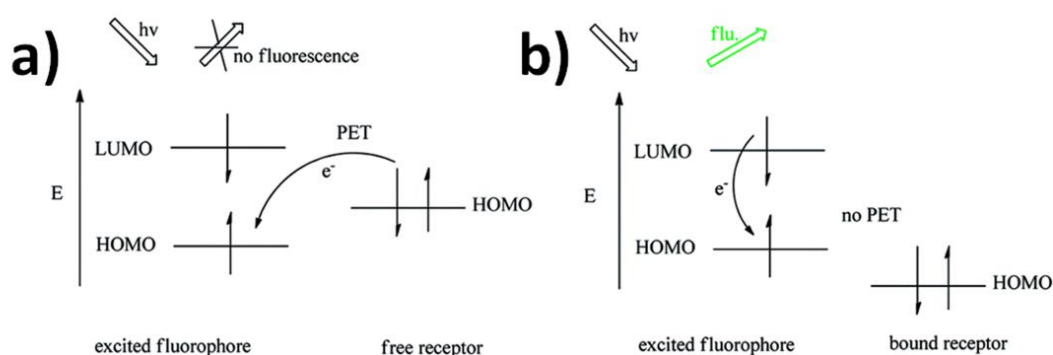


**Figure 1.9:** Energy diagram of fluorescent probe a) with PET and b) without PET [27]

### 1.3.2.2 Intramolecular charge transfer (ICT)

Intramolecular charge transfer (ICT) is a process in which fluorophore and receptor are connected through  $\pi$ -conjugation system. When receptor bind with analyte, the excited state of the whole molecule becomes more stable, resulting in narrowing its energy gap and releasing of red-shifted fluorescence (Figure 1.10).

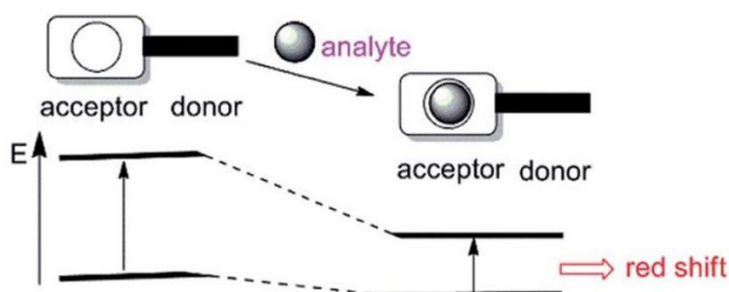


**Figure 1.10:** Energy diagram of fluorescent probe with ICT process [26]

### 1.3.2.3 Excited-state intramolecular proton transfer (ESIPT)

Upon excitation, receptor of the probe containing ketone or imine can undergo proton transfer through hydrogen bonding into enol form or keto form (Figure 1.11). Analyte prefer bonding with one of the two form, resulting in blue-shifted or red-shifted fluorescent signal.

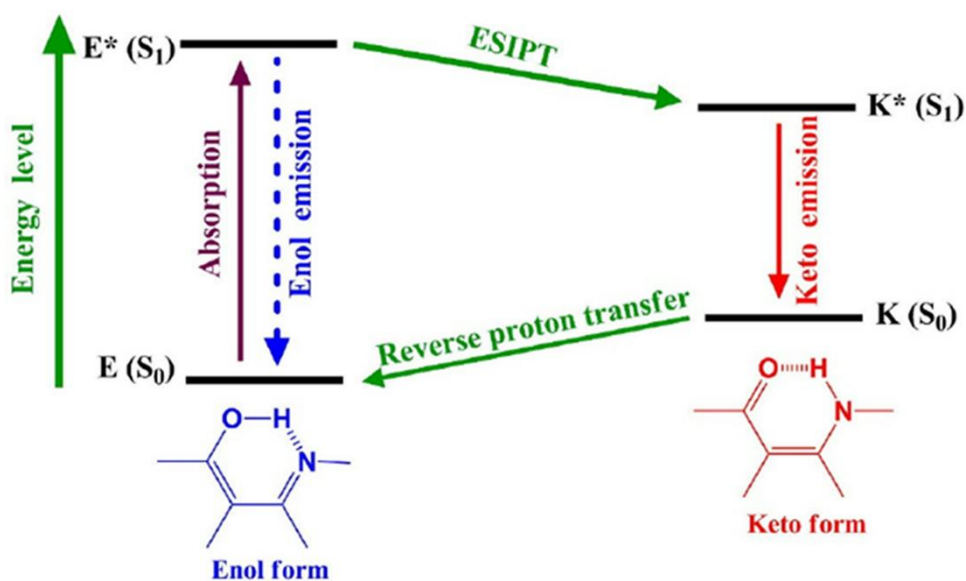


Figure 1.11: Energy diagram of fluorescent probe with ESIPT process [28]

### 1.3.2.4 Förster Resonance energy transfer (FRET)

Förster Resonance energy transfer (FRET) process occur in fluorescent probe containing two fluorophores. Emission spectrum of donor fluorophore overlap with absorption spectrum of acceptor fluorophore. The fluorescent energy released from donor fluorophore will be absorbed by the acceptor fluorophore, resulting in red-shifted fluorescent signal (Figure 1.12).

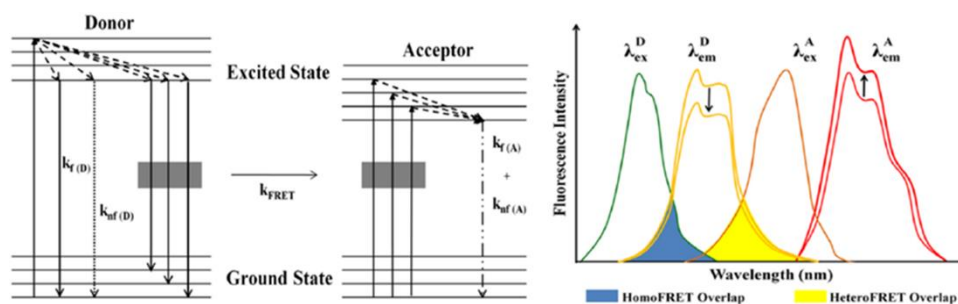


Figure 1.12: Energy diagram of fluorescent probe with FRET process [29]



### 1.3.3 Modes of fluorescent sensor

Fluorescent probe can be divided into three modes based on how its fluorescent signal changes including turn-on mode, turn-off mode and ratiometric mode (Figure 1.13).

#### 1.3.3.1 Turn-off mode

Turn-off mode provides fluorescent reduction upon addition of analyte caused by PET process. It usually requires initially high fluorescence intensity to get high sensitivity. However, limitation of this mode is it suffers from noise of instrument and fault positive result.

#### 1.3.3.2 Turn-on mode

Turn-on mode provides fluorescent enhancement upon addition of analyte. It usually requires suppression of initial fluorescence via PET process to get high sensitivity. This mode is popular and widely used due to high sensitivity.

#### 1.3.3.3 Ratiometric mode

Ratiometric mode provides change of fluorescence from one wavelength to another wavelength via ICT, ESIPT or FRET process. If the emissive wavelength becomes shorter, it is called blue-shift. If the emissive wavelength becomes longer, it's called red-shift. This mode has advantage on elimination of noise of instrument.

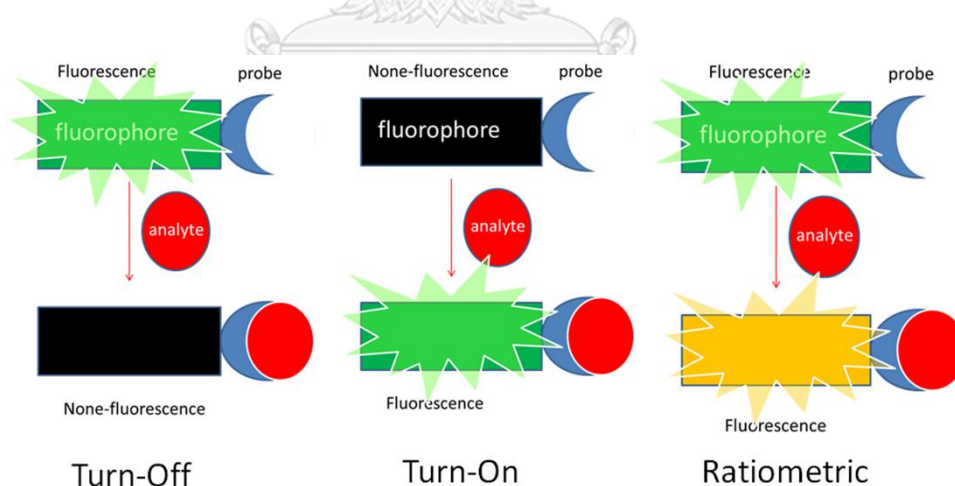


**Figure 1.13:** Modes of fluorescent sensor

## 1.4 Literature review

### 1.4.1 Review on Fluorescent probes for ROS detection

Based on mechanism of fluorescent signal change, many fluorescent probes have been developed for ROS detection. As we described the benefit above, most of recent works have been designed and developed as turn-on fluorescent probes

In 2004, Chang et al. [15] have developed a fluorescein-based probe **PF1** containing boronate unit. The probe could response toward  $\text{H}_2\text{O}_2$  in 20 mM HEPES buffer solution pH 7 or HEK cells, resulting in enhancement of green emission (Figure 1.14).

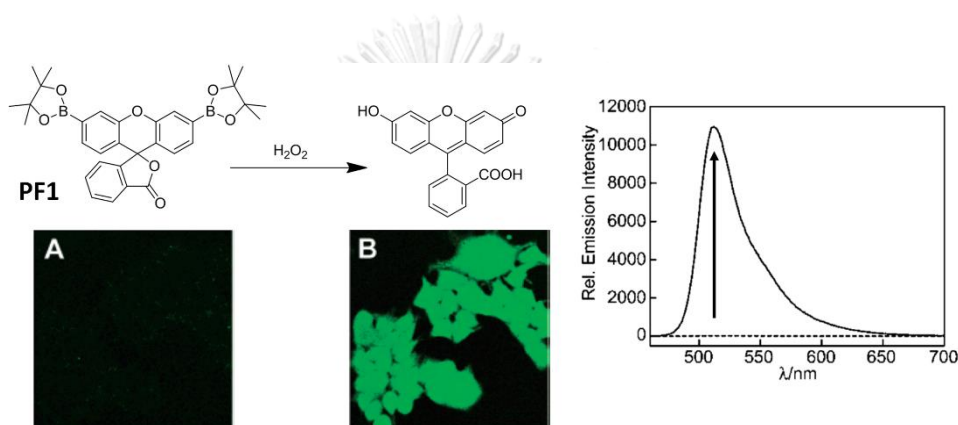


**Figure 1.14:** Reaction of probe 1 toward  $\text{H}_2\text{O}_2$

In 2013, Long et al. [30] synthesized a fluorescent sensor **HRS1** based on dual fluorophores, rhodamine and coumarin. This sensor, which emitted only green fluorescence from coumarin unit, could be oxidized by  $\text{OCl}^-$  and then two fluorophores were separated from each other (Figure 1.15). Therefore, ratiometric fluorescent signal could be observed from **fluorophore 1** and **fluorophore 2** in red and blue, respectively. This sensor was selective to  $\text{OCl}^-$  over other ions and ROS with LOD of 24 nM and could be applied for the detection in real water samples.



**Figure 1.15:** Reaction of HRS1 with  $\text{OCl}^-$

In 2019, He et al. [31] have been developed a dicyanomethylene-4H-pyran derivative **DCHP** as fluorescent probe for detection of  $\text{H}_2\text{O}_2$ . This probe displayed red turn-on fluorescence at 653 nm upon addition of  $\text{H}_2\text{O}_2$  with LOD of  $5.3 \mu\text{M}$ . This probe could also be applied in cell-imaging (Figure 1.16).

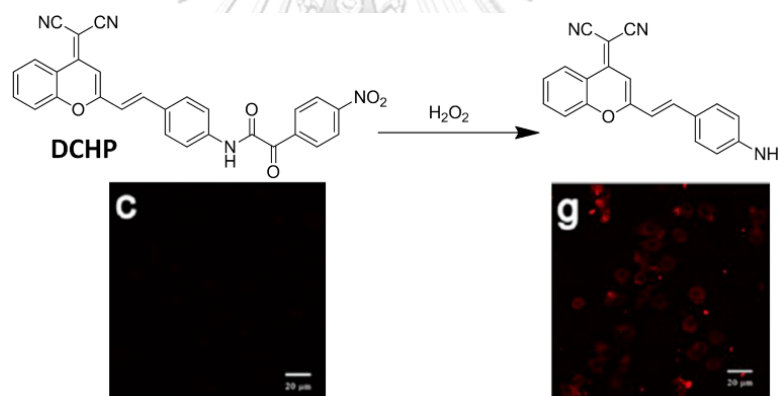


**Figure 1.16:** Response of **DCHP** toward  $\text{H}_2\text{O}_2$

#### 1.4.2 Review on BODIPY-based fluorescent probes for ROS detection

In 2011, Kim et al. [32] synthesized methylthio-BODIPY **7** which emitted red fluorescence due to electron-donating substituent. Upon addition of ROS, electron-donating thioether was oxidized into electron-withdrawing sulfoxide which underwent blue-shifted emission. This caused the ratiometric change from red to green fluorescence (Figure 1.17) which was also compatible for cells imaging.

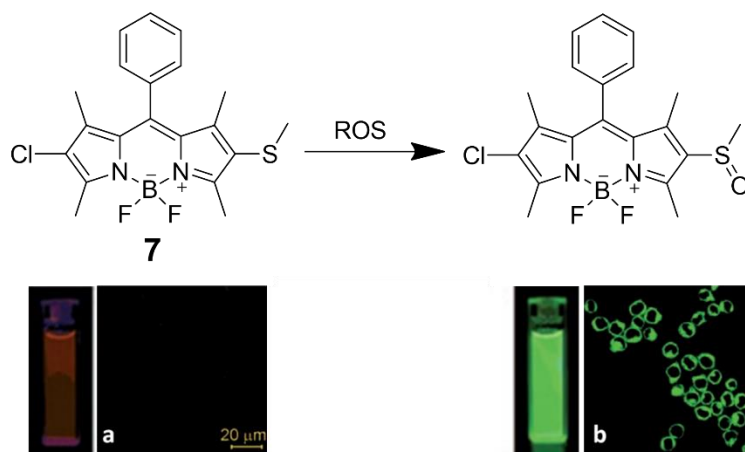


**Figure 1.17:** Ratiometric sensing of probe **7** toward ROS

In 2017, Lei et al. [33] have developed a BODIPY-based fluorescent probe **OHP** containing dichloromethyl group. This probe could selectively response toward OH radical, resulting in turn-off green fluorescence at 514 nm. Limit of detection was determined to be 11 nM. This probe could also detect exogenous  $\bullet\text{OH}$  in live cells (Figure 1.18).

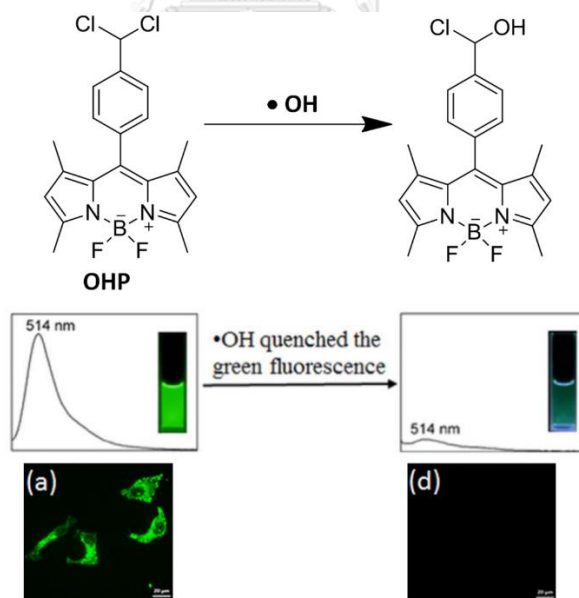


**Figure 1.18:** Response of probe **OHP** toward  $\bullet\text{OH}$

In the same year, Xu and Qian [34] have developed a fluorescent probe **OX-PPA-BODIPY** containing oxime group as a receptor. This probe could be hydrolyzed by  $\text{ClO}^-$  to

generate aldehyde product which provided strong green fluorescence (Figure 1.19). This probe could be applied in real water sample.

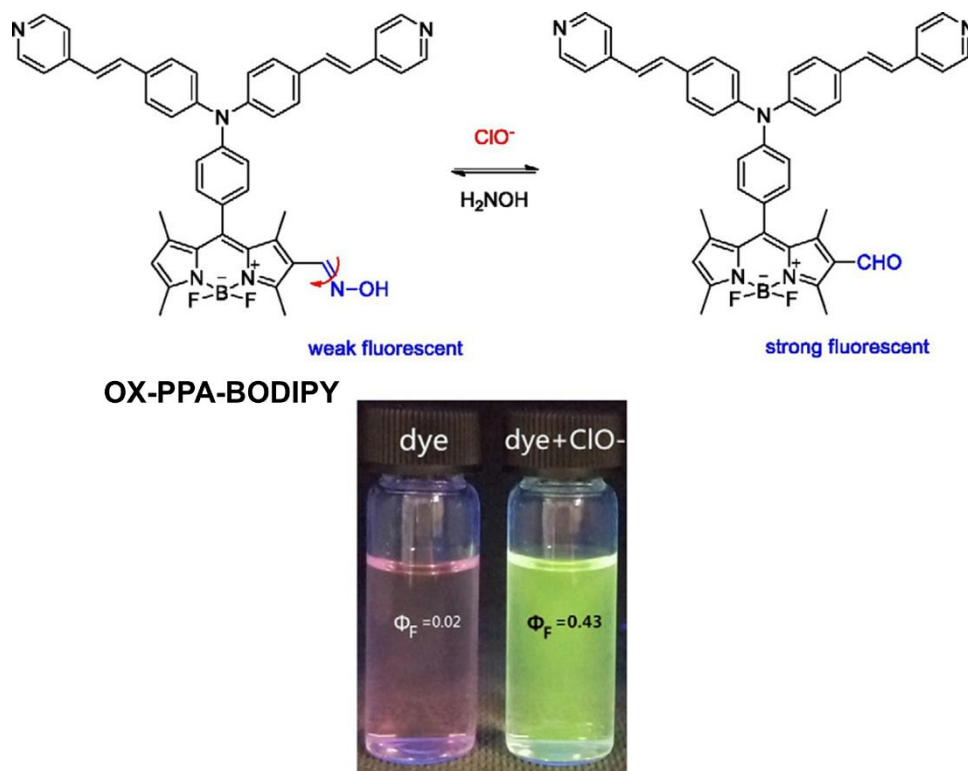


**Figure 1.19:** Response of probe **OX-PPA-BODIPY** toward  $\text{ClO}^-$

In 2019, Xu and Qian [35] have developed BODIPY-based fluorescent probe **BODIPY-SE** containing selenide unit. Selenide moiety could be oxidized by  $\text{H}_2\text{O}_2$  into selenoxide, resulting in inhibition of PET effect and then turn-on green fluorescence (Figure 1.20). This probe could be applied for exogenous  $\text{H}_2\text{O}_2$  in live cells.

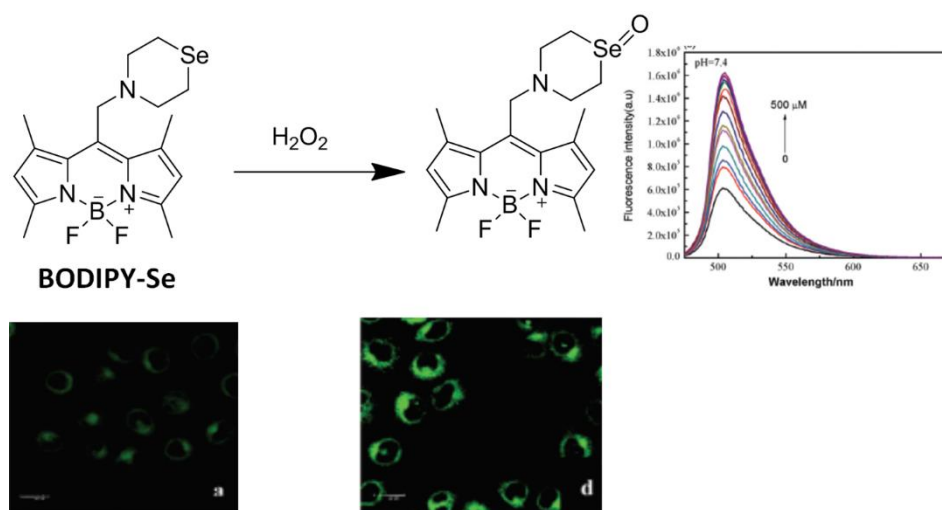


**Figure 1.20:** Response of **BODIPY-Se** toward  $\text{H}_2\text{O}_2$

## 1.5 Introduction of gold species

### 1.5.1 Basic of gold species

Gold is an element with symbol of Au and atomic number 79 in the transition metal category on the periodic table. It is one of the least reactive metal and very rare in nature, hence the well-known precious metal used for jewelry and arts. Gold in pure solid form is insoluble in water. However, it can be suspended in water in the form of gold nanoparticle (AuNP). Moreover, gold compound, which commonly has oxidation state of +3 or in the Au(III) form, can be easily dissolved in aqueous solution.

### 1.5.2 Role of gold in organic reaction

Due to strong affinity toward alkynyl group, thiol group and other heteroatoms, gold can be used as a catalyst to activate those functional groups [36] which is summarized in Figure 1.21. Barluenga et al. [37] used  $\text{AuCl}_3$  as Lewis acid to activate alkynyl group for intramolecular cyclisation (Figure 1.21a). Later,  $\text{AuCl}_3$  was used to facilitate Friedel-Craft reaction between indole and styrene [38] (Figure 1.21b). Corma and Serna [39] used supported Au(0) as a catalyst for hydrogenation of nitro compound into aniline compound in the presence of  $\text{H}_2$  gas (Figure 1.21c). Lastly, Deng et al. [19] successfully performed oxidation of styrene into various oxidative products in the presence of  $\text{O}_2$  gas covered on gold surface (Figure 1.21d).

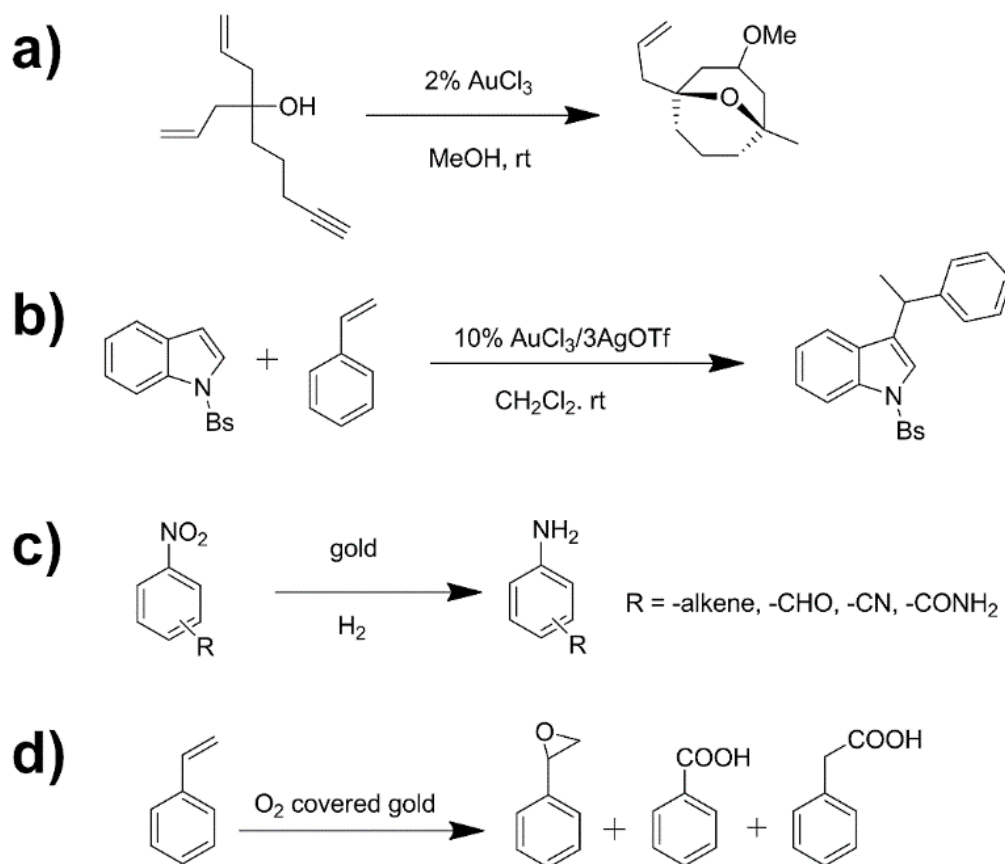


**Figure 1.21:** Gold-catalyzed organic transformations

## 1.6 Design of our fluorescent probes

Based on literature review of BODIPY-based fluorescent probes, there were mostly green emissive probes. However, in cell-imaging application, green-emissive probes may suffer from cell autofluorescence. Also, requirement of high excitation energy for monitoring the probe may result in damaging the living cells. Therefore, development of red-emissive probe is within our interest. Based on reaction between styrene and oxygen gas mentioned earlier (Figure 1.21d), it is possible to create a new and highly sensitive receptor for ROS detection. In this work, we therefore designed BODIPY-based fluorescent probe containing styryl moiety at 3- and 5-position for ROS detection (Figure 1.22). This aspect should extend  $\pi$ -conjugation and turn emissive wavelength of BODIPY from green into red region. Moreover, the styryl group could be oxidized by ROS with the help of gold ion, allowed us to monitor amount of ROS by the change in fluorescent intensity of our designed probe.

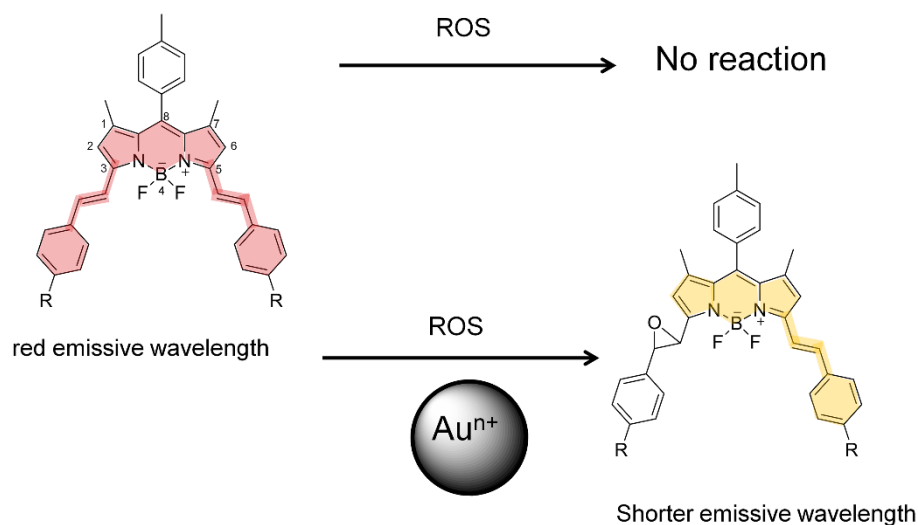


**Figure 1.22:** Design of styryl-BODIPY probes and hypothesis on gold-catalyzed oxidation

### 1.7 Objective of this research

1. To synthesize four red-emissive BODIPY-based fluorescent probes (Figure 1.23) containing tolyl (**SB1**), phenolic (**SB2**), catechol (**SB3**) and salicylic group (**SB4**) to investigate substituent effect on photophysical properties and responsive ability toward ROS.

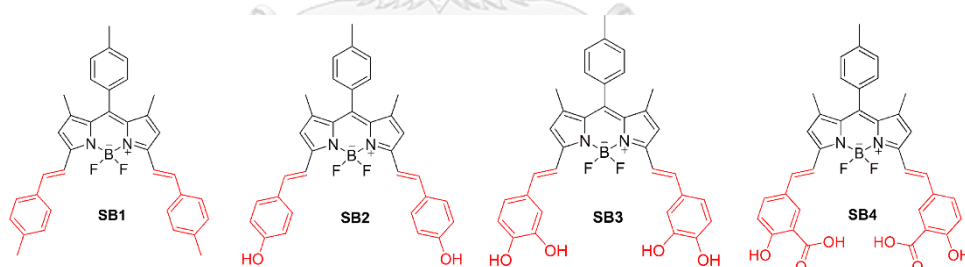


**Figure 1.23:** Chemical structure of the probes **SB1–4**

2. To select the best probe and optimized condition for detection of ROS.
3. To apply the probe for detection of exogenous and endogenous ROS in live cell.



## CHAPTER II EXPERIMENTAL

### 2.1. Materials

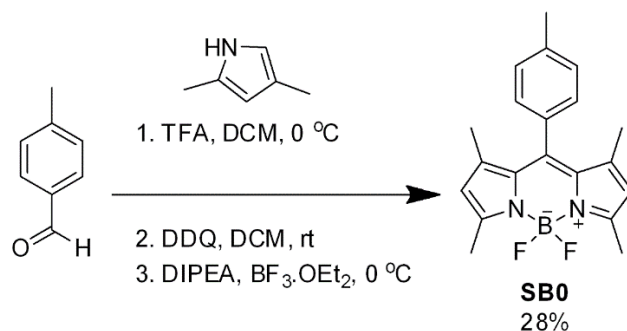
All reagents were purchased from RCI Labscan, Sigma-Aldrich, TCI, Merck, Fluka, Chemieliva, AnalaR, Loba chemie, Carlo Erba or Invitrogen (Grand Island, NY, USA) and used without further purification. Column chromatography was carried out with silica gel (60, 230–400 mesh) from ICN Silitech. Analytical thin-layer chromatography (TLC) was performed on Kieselgel F-254 pre-coated plastic TLC plates from EM Science. Visualization of the products on TLC was observed under 254 nm and 365 nm ultraviolet lamp.

### 2.2. Analytical instruments

Mass spectra were obtained from Microflex MALDI-TOF mass spectrometer (Bruker Daltonics) using doubly recrystallized 2-cyano-4-hydroxycinnamic acid (CCA) as a matrix. Electrospray ionization high-resolution mass spectra (ESI-HRMS) were obtained from Micromass Quattro micro TM API (Waters, USA). NMR spectra were obtained from Varian Mercury NMR spectrometer operating at 400 MHz for  $^1\text{H}$ -NMR and 100 MHz for  $^{13}\text{C}$ -NMR (Varian Company, CA, USA). Absorption and emission spectra were obtained from Cary100Bio UV–Visible spectrophotometer and Carry Eclipse fluorescence spectrophotometer (Agilent Technologies) using 10×10 mm quartz cuvette (Starna Scientific). Confocal microscopic images were taken by Fluoroview FV10i confocal laser microscope. The pH of each sample solution was measured by Ohaus Starter2001 pH meter.

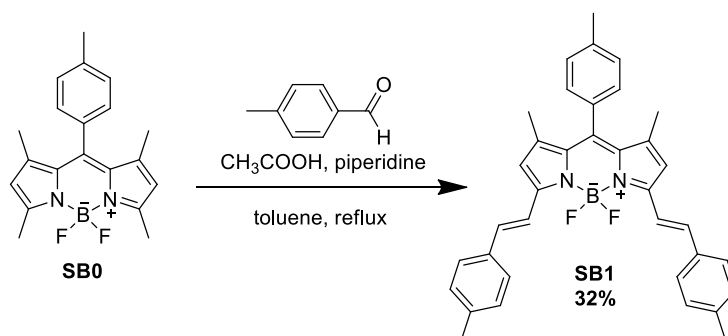
### 2.3. Synthesis of BODIPY probes

#### 2.3.1. Precursor **SB0**

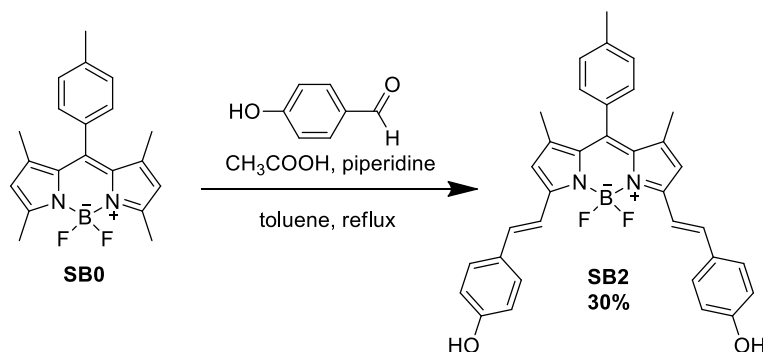


**Figure 2.24:** preparation of SB0

2,4-dimethylpyrrole (2.009 g, 21.1 mmol) and tolualdehyde (1.015 g, 8.4 mmol) were dissolved in dry dichloromethane (DCM, 100 mL). The solution was stirred by magnetic bar in round-bottom flask at 0 °C under N<sub>2</sub> atmosphere for 5 minutes. The solution was added with a few drops of trifluoroacetic acid (TFA) and stirred for another 2 hours. Then the reaction mixture was quenched with saturated NaHCO<sub>3</sub> (aq, 20 mL) followed by washing three times (3×20 mL) with deionized water. The organic layer was dried over Na<sub>2</sub>SO<sub>4</sub> and evaporated under reduced pressure. The crude was purified by column chromatography using silica gel as stationary phase and ethyl acetate/hexane (1/9 v/v) as mobile phase. The oil product was diluted in dry DCM (100 mL). 2,3-Dichloro-5,6-dicyano-1,4-benzoquinone (DDQ, 1.719 g, 7.6 mmol) was added to the solution in round-bottom flask. The reaction was stirred under N<sub>2</sub> atmosphere at room temperature (rt) for 30 minutes. Then the flask was cooled in ice bath. BF<sub>3</sub>•OEt<sub>2</sub> (9.3 mL, 75.4 mmol) and *N,N*-Diisopropylethylamine (DIPEA, 9.2 mL, 52.8 mmol) were added to the reaction. The reaction was stirred overnight. The reaction mixture was quenched with saturated NaHCO<sub>3</sub> (20 mL) followed by washing three times (3×20 mL) with saturated NaCl. The organic layer was dried over Na<sub>2</sub>SO<sub>4</sub> and evaporated under reduced pressure. The crude was purified by column chromatography using silica gel as stationary phase and ethyl acetate/hexane (1/9 v/v) as mobile phase. The product was obtained as orange solid (811 mg, isolated yield: 28%). <sup>1</sup>H NMR (400 MHz, CDCl<sub>3</sub>): δ = 7.22–7.20 (d, *J* = 8 Hz, 2H), 7.08–7.06 (d, *J* = 8 Hz, 2H), 5.90 (s, 2H), 2.48 (s, 6H), 2.36 (s, 3H), 1.32 (s, 6H). <sup>13</sup>C NMR (CDCl<sub>3</sub>): δ = 155.2, 143.2, 142.2, 138.8, 132.0, 131.6, 129.8, 127.8, 121.1, 29.7, 21.4, 14.4. ESI-HRMS (*m/z*): [M+Na]<sup>+</sup> calculated for C<sub>20</sub>H<sub>21</sub>BF<sub>2</sub>N<sub>2</sub>Na: 361.1664, found 361.1661.

2.3.2. Probe **SB1**Figure 2.25: Preparation of **SB1**

**SB0** (33.4 mg, 0.1 mmol), dry toluene (20 mL), tolualdehyde (0.1 mL, 0.8 mmol), acetic acid (1.4 mL) and piperidine (1.4 mL) were mixed together in round-bottom flask, equipped with reflux condenser. The mixture was stirred overnight under  $\text{N}_2$  atmosphere at reflux temperature (110 °C). After cooling to rt, the reaction was quenched with saturated  $\text{NaHCO}_3$  (20 mL) followed by extraction three times ( $3 \times 20$  mL) with DCM. The organic layers were combined, washed three times ( $3 \times 20$  mL) with deionized water, dried over  $\text{Na}_2\text{SO}_4$  and evaporated under reduced pressure. The crude was purified by column chromatography using silica gel as stationary phase and ethyl acetate/hexane (1/4 v/v) as mobile phase. The product was obtained as dark blue solid (17.4 mg, isolated yield: 32%).  $^1\text{H}$  NMR (400 MHz,  $\text{CDCl}_3$ ):  $\delta$  = 7.74–7.70 (d,  $J$  = 16 Hz, 2H), 7.57–7.55 (d,  $J$  = 8 Hz, 4H), 7.33–7.22 (m, 10H), 6.65 (s, 2H), 2.48 (s, 3H), 2.41 (s, 6H), 1.49 (s, 6H).  $^{13}\text{C}$  NMR ( $\text{CDCl}_3$ ):  $\delta$  = 152.6, 142.0, 139.1, 138.8, 136.0, 134.0, 133.5, 132.2, 129.7, 129.5, 128.3, 127.5, 118.5, 117.6, 29.7, 21.4, 14.7. ESI-HRMS ( $m/z$ ):  $[\text{M}+\text{H}]^+$  calculated for  $\text{C}_{36}\text{H}_{34}\text{BF}_2\text{N}_2$ : 543.2783, found 543.2787.

2.3.3. Probe **SB2**Figure 2.26: Preparation of **SB2**

**SB0** (50 mg, 0.15 mmol), dry toluene (9 mL), para-hydroxybenzaldehyde (144 mg, 1.2 mmol), acetic acid (0.4 mL) and piperidine (0.9 mL) were mixed together in round-bottom flask, equipped with reflux condenser. The mixture was stirred overnight under N<sub>2</sub> atmosphere at refluxed temperature (110 °C). After cooling to rt, the reaction was quenched with deionized water (20 mL), acidified by a few drops of concentrated HCl and extracted three times (3×20 mL) with ethyl acetate. The organic layers were combined, dried over Na<sub>2</sub>SO<sub>4</sub> and evaporated under reduced pressure. The crude was purified by column chromatography using silica gel as stationary phase and MeOH/DCM (1/99 v/v) as mobile phase. The product was obtained as dark blue solid (24.1 mg, isolated yield: 30%). <sup>1</sup>H NMR (400 MHz, acetone-D<sub>6</sub>): δ = 7.47–7.42 (d, *J*=20 Hz, 2H), 7.42–7.40 (d, *J* = 8 Hz, 4H), 7.33–7.31 (d, *J*=8 Hz, 2H), 7.31–7.29 (d, *J* = 8 Hz, 2H), 7.20–7.18 (d, *J* = 8 Hz, 2H), 6.83–6.81 (d, *J* = 8 Hz, 4H), 6.69 (s, 2H), 2.33 (s, 3H), 1.35 (s, 6H). <sup>13</sup>C NMR (DMSO-D<sub>6</sub>): δ = 158.9, 152.2, 141.2, 138.5, 137.9, 136.8, 132.5, 131.4, 129.6, 129.0, 128.2, 127.4, 117.8, 116.1, 115.1, 20.9, 14.3. ESI-HRMS (*m/z*): [M]<sup>+</sup> calculated for C<sub>34</sub>H<sub>29</sub>BF<sub>2</sub>N<sub>2</sub>O<sub>2</sub>: 546.2290, found 546.2148.

#### 2.3.4. Probe **SB4**

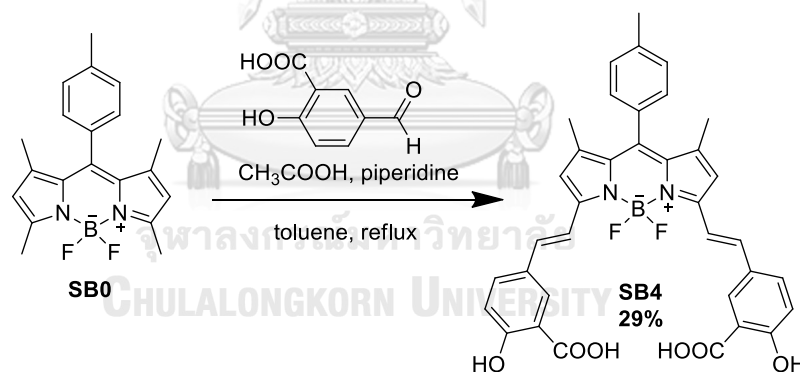


**Figure 2.27:** Preparation of **SB4**

**SB0** (51.4 mg, 0.152 mmol), dry toluene (4 mL), 5-formylsalicylic acid (204.7 mg, 1.23 mmol), acetic acid (0.5 mL) and piperidine (1.0 mL) were mixed together in round-bottom flask, equipped with reflux condenser. The mixture was stirred overnight under N<sub>2</sub> atmosphere at refluxed temperature (110 °C). After cooling to rt, the reaction was quenched with deionized water (20 mL), acidified by a few drops of concentrated HCl and extracted three times (3×20 mL) with ethyl acetate. The organic layers were combined, dried over Na<sub>2</sub>SO<sub>4</sub> and evaporated under reduced pressure. The crude was purified by recrystallization using hexane and ethyl acetate. The

product was obtained as dark blue solid (27.7 mg, isolated yield: 29%).  $^1\text{H}$  NMR (400 MHz, DMSO- $\text{D}_6$ ):  $\delta$  = 8.02 (s, 2H), 7.83–7.81 (d,  $J$  = 8 Hz, 2H), 7.61–7.57 (d,  $J$  = 16 Hz, 2H), 7.41–7.37 (dd,  $J$  = 16 Hz, 4H), 7.32–7.30 (d,  $J$  = 8 Hz, 2H), 7.08–7.06 (d,  $J$  = 8 Hz, 2H), 6.95 (s, 2H), 2.43 (s, 3H), 1.44 (s, 6H).  $^{13}\text{C}$  NMR (DMSO- $\text{D}_6$ ):  $\delta$  = 175.5, 164.3, 154.2, 143.1, 140.4, 137.6, 134.3, 133.6, 132.3, 131.7, 130.9, 129.8, 128.4, 120.5, 118.6, 118.2, 117.3, 23.8, 23.1, 21.4, 14.9. ESI-HRMS ( $m/z$ ):  $[\text{M}-\text{H}]^-$  calculated for  $\text{C}_{36}\text{H}_{28}\text{BF}_2\text{N}_2\text{O}_6$ : 633.2014, found 632.9846.

#### 2.4. Preparation of ROS and metal ions

$\text{NaOCl}$ ,  $\text{H}_2\text{O}_2$ ,  $^t\text{BuOOH}$  and metal ions were commercially used and diluted in milliQ water without further purification. Concentration of  $\text{NaOCl}$  was determined by UV-vis spectrophotometer using an extinction coefficient of  $350 \text{ M}^{-1}\text{cm}^{-1}$  at 292 nm. Singlet oxygen ( $^1\text{O}_2$ ) was generated *in situ* by the addition of  $\text{Na}_2\text{MoO}_4 \cdot 2\text{H}_2\text{O}$  and  $\text{H}_2\text{O}_2$  [40]. Hydroxyl radical ( $\bullet\text{OH}$ ) was generated *in situ* by the addition of  $(\text{NH}_4)_2\text{Fe}(\text{SO}_4)_2 \cdot 6\text{H}_2\text{O}$  and  $\text{H}_2\text{O}_2$ .

#### 2.5. Cell culture

The murine macrophage cell line RAW264.7 (ATCC number TIB-71) was purchased from American Type Culture Collection, ATCC (Bethesda, MD, USA). Cells were cultured in Dulbecco's Modified Eagle Medium (DMEM) supplemented with 10% heat-inactivated Fetal Bovine Serum (FBS), 100 units/mL of penicillin, and 100  $\mu\text{g}/\text{mL}$  of streptomycin at 37 °C in a humidified atmosphere of 5%  $\text{CO}_2/95\%$  air.

#### 2.6. Cytotoxicity of SB2 on RAW264.7 cells

Cytotoxicity of **SB2** on RAW264.7 cells was evaluated prior to use as **SB2** as a dye for antioxidant activity evaluation. Cells were seeded in 24-well plates at a density of  $1.7 \times 10^4$  cells/500  $\mu\text{L}$  complete medium/well and incubated at 37 °C in a humidified atmosphere at 95% air/5%  $\text{CO}_2$  for 24 h. Culture cells were divided into six groups; cells treated with 1% MeOH as a control group, cells treated with lipopolysaccharide (LPS) only, cells treated with **SB2** at concentration 1 or 10  $\mu\text{M}$ , and cells treated with LPS plus **SB2** at concentration 1 or 10  $\mu\text{M}$ . Control and treated culture cells were washed and added with DMEM. In the LPS-induced group, LPS was added at final concentration 1  $\mu\text{g}/\text{mL}$  for 18 h and the induced cells were washed and

added with DMEM. Solutions of **SB2** in MeOH at two different concentrations was added to the cells and further incubated for 30 minutes. Treated cells were washed and added with DMEM. 3-(4,5-dimethylthiazol-2-yl)-2,5-diphenyltetrazolium bromide (MTT) was then added at a final concentration 0.5 mg/mL and further incubated for 4 h. The media was removed and DMSO was then added to dissolve formazan crystals. The absorbance of formazan was measured at 540 nm using a microplate reader (CLARIOstar, BMG LABTECH, Germany). Five replicates were performed.

## 2.7. Cells imaging

### 2.7.1. **SB2**-stained cells

Cells were placed on 8-well chambers and cultured in DMEM (400  $\mu$ L for each well) for one day. The cells in each chamber were incubated with **SB2** in MeOH (final concentration: 1  $\mu$ M **SB2**, 1% MeOH in DMEM) at 37  $^{\circ}$ C for 30 minutes. The stained cells were washed three time (3 $\times$ 200  $\mu$ L for each well) with phosphate buffer saline (PBS, 0.1 M) to remove remaining **SB2**.

### 2.7.2. Exogenous NaOCl

After cells were incubated with **SB2** and washed with PBS as described in 2.7.1, DMEM (400  $\mu$ L) was added, followed by NaOCl in water (final concentration: 1, 2.5 or 10  $\mu$ M). The samples were incubated at 37  $^{\circ}$ C for 30 minutes and then washed three times (3 $\times$ 200  $\mu$ L for each well) with PBS (0.1 M) to remove remaining NaOCl.

### 2.7.3. Endogenous ROS

After cells were cultured in DMEM for one day as described in 2.7.1, the cells were incubated with LPS (final concentration: 0.1, 1, 2.5 or 10  $\mu$ g/mL) at 37  $^{\circ}$ C for 18 hours. The treated cells were washed three times (3 $\times$ 200  $\mu$ L for each well) with PBS (0.1 M) to remove remaining LPS. Then the samples were incubated with **SB2** as described in 2.7.1.

### 2.7.4. Samples preparation for confocal laser microscopy

After cells were incubated with **SB2** and ROS, the cells were fixed by 4% paraformaldehyde in PBS solution at 37  $^{\circ}$ C for 10 minutes. Then the solution was removed. Mowiol (a contrast agent) was dropped on each sample. Then samples were covered with cover slide. Fluorescent signal from each sample was recorded by confocal laser microscope ( $\lambda_{\text{ex}}$  = 559 nm,  $\lambda_{\text{em}}$  = 570–620 nm).

## Chapter III RESULTS AND DISCUSSION

### 3.1 Synthesis of probes SB1–4

In this research, four fluorescent probes were designed based on BODIPY, **SB1–4**, and their structures are shown in Figure 3.28. Synthesis procedure of each probe is described thoroughly in section 2.3 and we also summarized synthetic method in Figure 3.29. Firstly, tolualdehyde was condensed with 2,4-dimethylpyrrole catalyzed by trifluoroacetic acid (TFA). The purified product was oxidized by 2,3-dichloro-5,6-dicyano-1,4-benzoquinone (DDQ), followed by complexation with  $\text{BF}_3$  to obtain precursor **SB0** (28% isolated yield). **SB0** was reacted with corresponding aldehydes via Knoevenagel condensation to afford **SB1**, **SB2** and **SB4** in 32%, 30% and 29% yield, respectively. Unfortunately, synthesis of **SB3** was unsuccessful. Due to its high affinity on silica gel, **SB3** could not be flushed out of column chromatography.

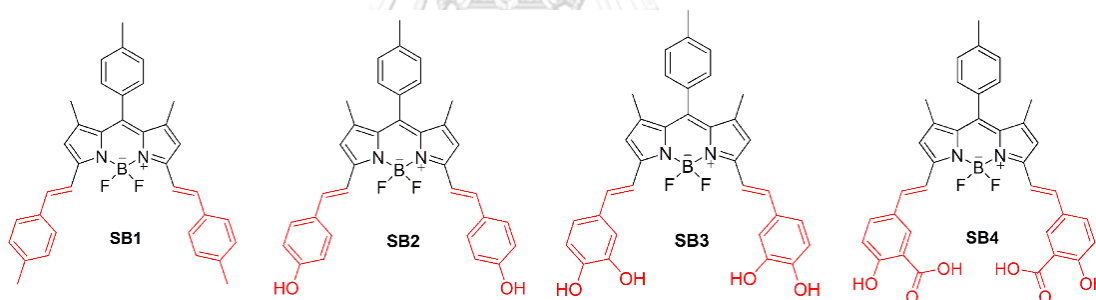
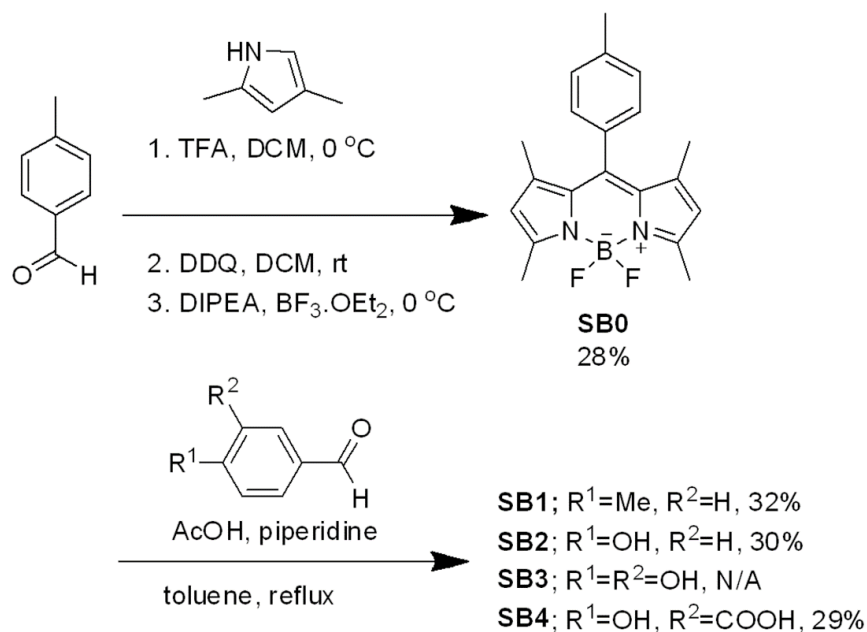


Figure 3.28: Chemical structure of probes SB1–4



**Figure 3.29:** Preparation of probes **SB1–4**

The structures of **SB1**, **SB2** and **SB4** were confirmed by <sup>1</sup>H-NMR spectra in comparison with **SB0** (Figure 3.30). Signals of proton a–e were found in all probes. However, a signal of proton f at 2.5 ppm in **SB0** disappeared in **SB1**, **SB2** and **SB4** spectra confirming successful Knoevenagel condensations. Moreover, new peaks were observed at aromatic region (6.5–8.0) in **SB1**, **SB2** and **SB4** spectra corresponding to the styryl moieties. These results confirmed the structures of **SB1**, **SB2** and **SB4**. Each probe was also confirmed by <sup>13</sup>C-NMR and ESI-HRMS (Appendix, Figure A.48–59).



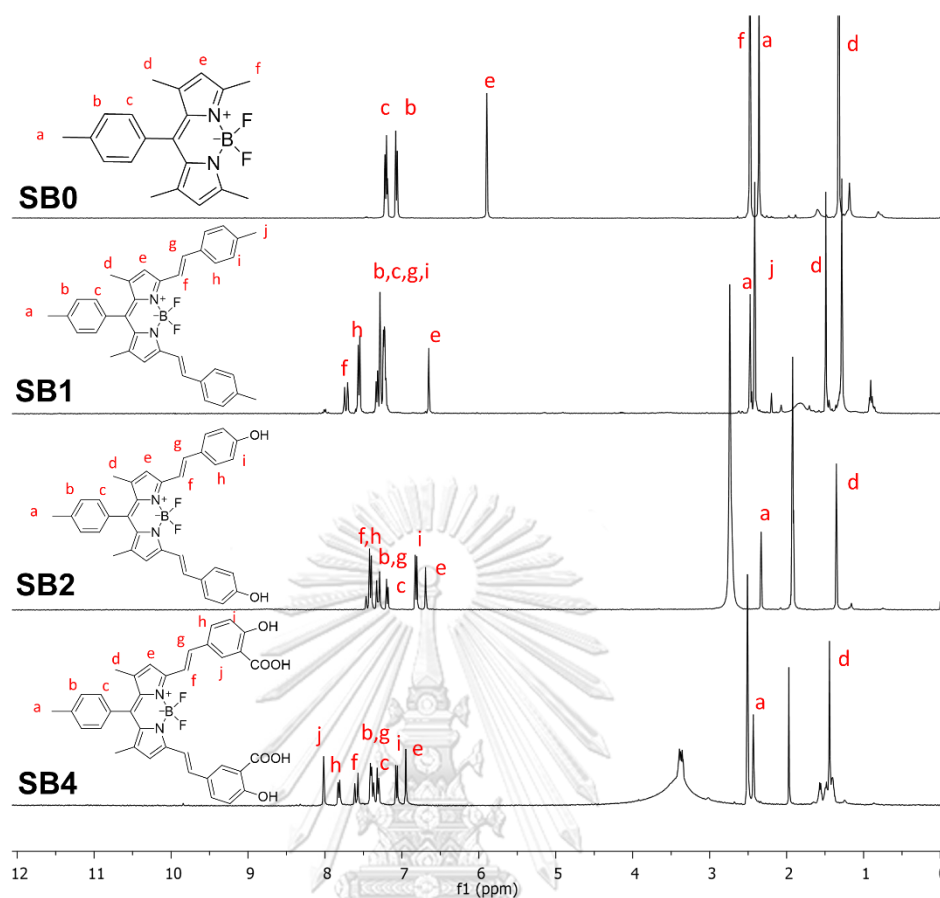
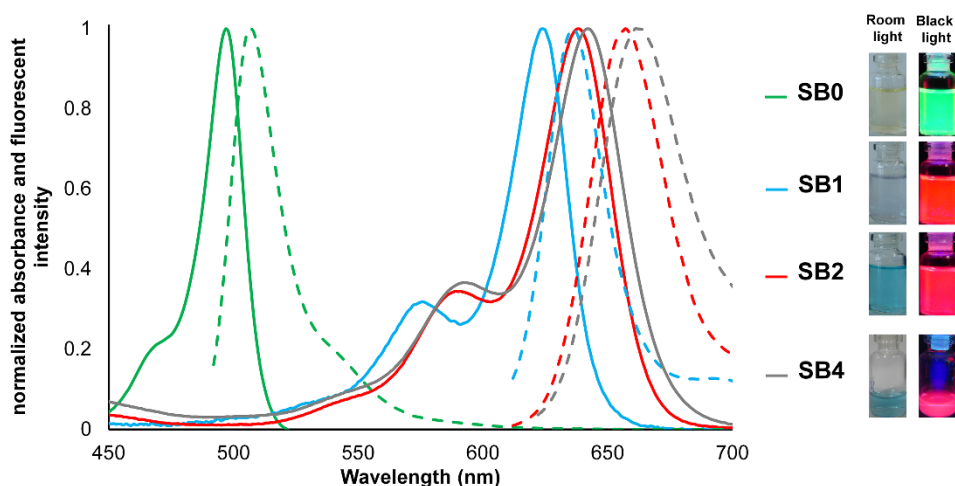


Figure 3.30:  $^1\text{H-NMR}$  spectra of **SB0**, **SB1**, **SB2** and **SB4**

### 3.2 Photophysical properties of **SB0**, **SB1**, **SB2** and **SB4**

Photophysical properties of four probes including **SB0**, **SB1**, **SB2** and **SB4** were measured by spectrophotometry in methanol. Their absorption and emission spectra are shown in Figure 3.31 and their photophysical properties are summarized in Table 3.1. The maximum absorption and emission wavelength of **SB0** were at 497 nm and 507 nm, respectively, which corresponded to pale orange color under room light and green fluorescence under black light. On the other hand, **SB1**, **SB2** and **SB4** absorbed at significantly longer wavelengths ( $\lambda_{\text{Ab}} \sim 624\text{--}642$  nm, blue color) and emitted red fluorescence ( $\lambda_{\text{Em}} \sim 634\text{--}662$  nm) under black light. This is due to the extended  $\pi$ -conjugation from styryl moieties as designed. Quantum yield of the three probes were estimated using zinc phthalocyanine as standard. We found that **SB2** and **SB4** gave significantly lower quantum yield than **SB1**. This result is perhaps caused by PET effect from

para-hydroxy group on styryl moiety toward the BODIPY core. Importantly, such low quantum yields of **SB2** and **SB4** make them potential useful as turn-on fluorescent probes.



**Figure 3.31:** Absorption (bold line) and emission (dash line) spectra of **SB0**, **SB1** and **SB2**, inset: Images of **SB0**, **SB1**, **SB2** and **SB4** in MeOH under room light and black light.

**Table 3.1** Photophysical properties of **SB0**, **SB1**, **SB2** and **SB4** in MeOH

Dye	$\lambda_{Ab/Ex/Em}$ (nm)	Stokes shift (nm)	$\phi_F$	$\epsilon$ ( $M^{-1}cm^{-1}$ ) <sup>c</sup>
<b>SB0</b>	497/480/507	10	0.23 <sup>a</sup>	55,003
<b>SB1</b>	624/600/634	10	0.97 <sup>b</sup>	28,477
<b>SB2</b>	638/600/657	19	0.37 <sup>b</sup>	84,937
<b>SB4</b>	642/600/662	20	0.42 <sup>b</sup>	N/A

<sup>a</sup> Use fluorescein ( $\phi_F = 0.95$  in 0.1 M NaOH) as standard

<sup>b</sup> Use zinc phthalocyanine ( $\phi_F = 0.30$  in 1% pyridine/toluene) as standard

<sup>c</sup> Measure at maximum absorption wavelength

### 3.3 Response of **SB2** and **SB4** toward $Au^{3+}$

There are several organic reactions that have Au species as a catalyst including hydrolysis, cyclisation, desulfurization and oxidation [36] (Figure 3.32). Oxidation on double

bond of styrene via reactive oxygen species (ROS) is also among them [19, 41] (Figure 3.32d). From above literature, we therefore designed our BODIPY probes containing double bond in the hope that it will react with ROS under Au catalyst. With probes in hand from above section, we then first tested the response of **SB2** and **SB4** toward  $\text{Au}^{3+}$  and compared with other metal ions. The responses were monitored by UV-vis spectrophotometry (Figure 3.33). The results showed that maximum absorption wavelength of these probes was blue-shifted (Figure 3.33a and c) together with enhancement of fluorescence intensity at 590 nm for **SB2** (Figure 3.33b and Figure 3.34a) and 596 nm for **SB4** (Figure 3.33d and Figure 3.34b) upon the addition of  $\text{Au}^{3+}$ . Color of solution under room light changed from blue into purple along with fluorescence change from red into orange under black light (Figure 3.34b inset). However, **SB4** was affected by other metal ions, including  $\text{Cu}^{2+}$  and  $\text{Al}^{3+}$ . We observed color fading along with decrease of both absorption and emission. Therefore, **SB2** was selected as a potential fluorescent probe because of its high specificity.

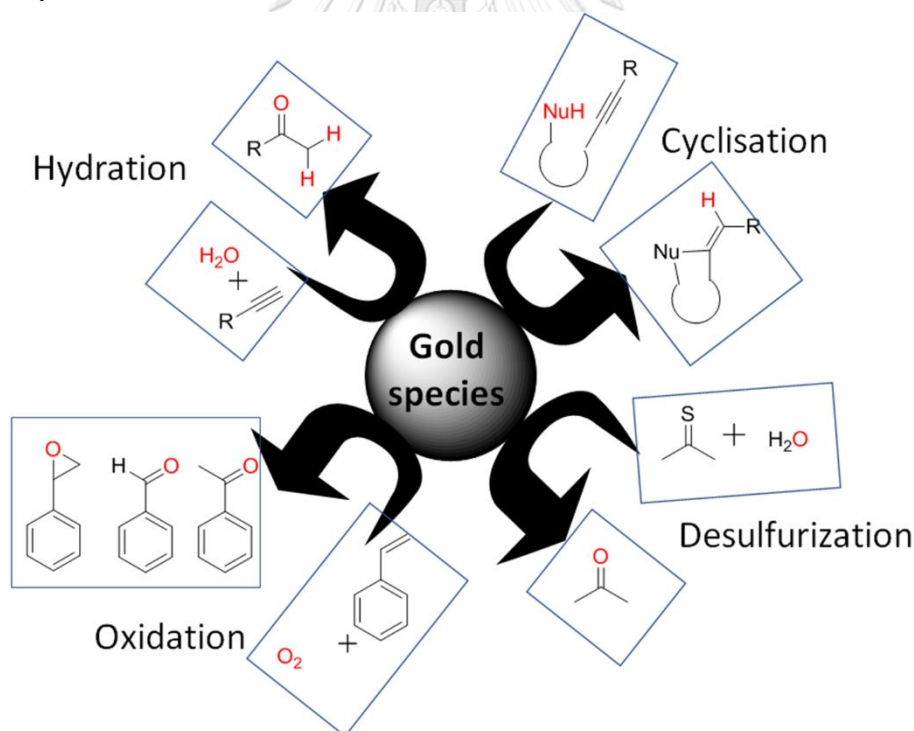


**Figure 3.32:** Gold-catalyzed organic transformations

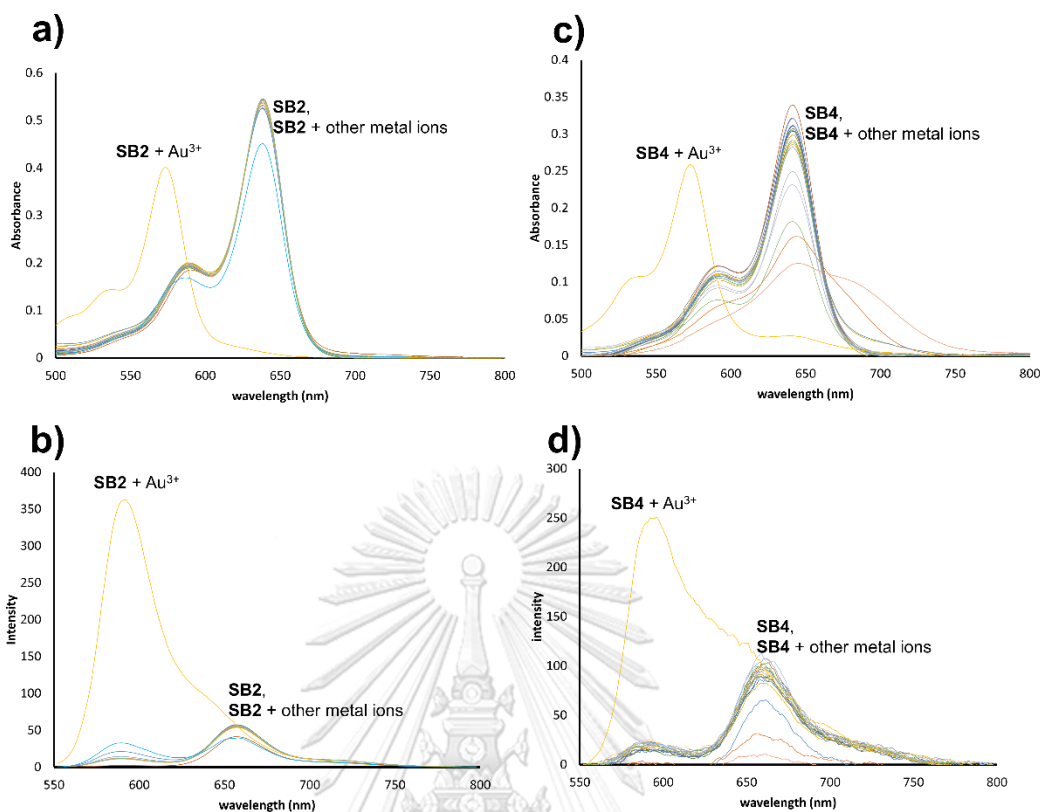


**Figure 3.33:** Absorption spectra (a,c), emission spectra (b,d;  $\lambda_{\text{Ex}} = 540 \text{ nm}$ ) of  $5 \mu\text{M}$  SB2 (a,b) and  $4 \mu\text{M}$  SB4 (c,d) in the presence of 10 equivalents metal ions including  $\text{Li}^+$ ,  $\text{Na}^+$ ,  $\text{K}^+$ ,  $\text{Mg}^{2+}$ ,  $\text{Ca}^{2+}$ ,  $\text{Ba}^{2+}$ ,  $\text{Al}^{3+}$ ,  $\text{Cr}^{3+}$ ,  $\text{Fe}^{2+}$ ,  $\text{Fe}^{3+}$ ,  $\text{Co}^{2+}$ ,  $\text{Ni}^{2+}$ ,  $\text{Cu}^{2+}$ ,  $\text{Zn}^{2+}$ ,  $\text{Pb}^{2+}$ ,  $\text{Hg}^{2+}$ ,  $\text{Cd}^{2+}$ ,  $\text{Ag}^+$  and  $\text{Au}^{3+}$ . All samples were measured after 1 hour of mixing in solution (4/1 v/v of MeOH/HEPES buffer pH 7).

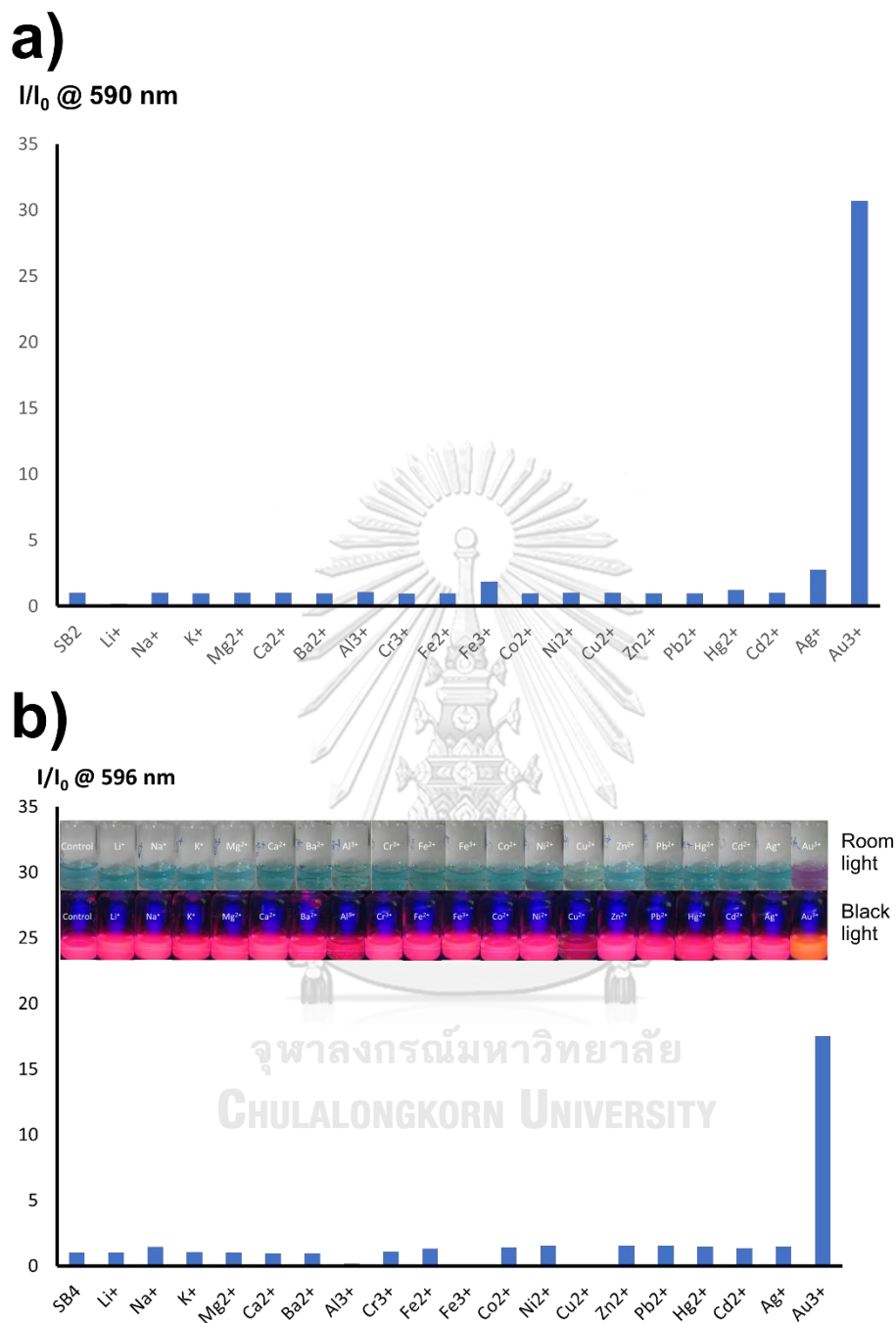


**Figure 3.34:** Fluorescence enhancement ratio ( $\lambda_{\text{Ex}} = 540 \text{ nm}$ ) of  $5 \mu\text{M}$  SB2 (a) and  $4 \mu\text{M}$  SB4 (b) in the presence of 10 equivalents metal ions including  $\text{Li}^+$ ,  $\text{Na}^+$ ,  $\text{K}^+$ ,  $\text{Mg}^{2+}$ ,  $\text{Ca}^{2+}$ ,  $\text{Ba}^{2+}$ ,  $\text{Al}^{3+}$ ,  $\text{Cr}^{3+}$ ,  $\text{Fe}^{2+}$ ,  $\text{Fe}^{3+}$ ,  $\text{Co}^{2+}$ ,  $\text{Ni}^{2+}$ ,  $\text{Cu}^{2+}$ ,  $\text{Zn}^{2+}$ ,  $\text{Pb}^{2+}$ ,  $\text{Hg}^{2+}$ ,  $\text{Cd}^{2+}$ ,  $\text{Ag}^+$  and  $\text{Au}^{3+}$ . Inset: image of solutions under room light and black light. All samples were measured after 1 hour of mixing in solution (4/1 v/v of MeOH/HEPES buffer pH 7).

Next, we applied **SB2** on biological samples. The RAW264.7 macrophage cell lines (white blood cells from mouse) were incubated with **SB2** for 30 minutes, followed by the addition of  $\text{Au}^{3+}$  for another 30 minutes. Confocal microscopic images of the cell samples in bright field dark field and merge are shown in Figure 3.35. There was no fluorescent signal at orange region (595 nm) from the cells before and after treatment with **SB2**. On the other hand, upon the addition of  $\text{Au}^{3+}$ , strong emission was observed in cytoplasm. These results suggested that **SB2** could penetrate through cell membrane to detect  $\text{Au}^{3+}$ . Moreover, this finding could possibly apply **SB2** as a probe for ROS detection in cells.

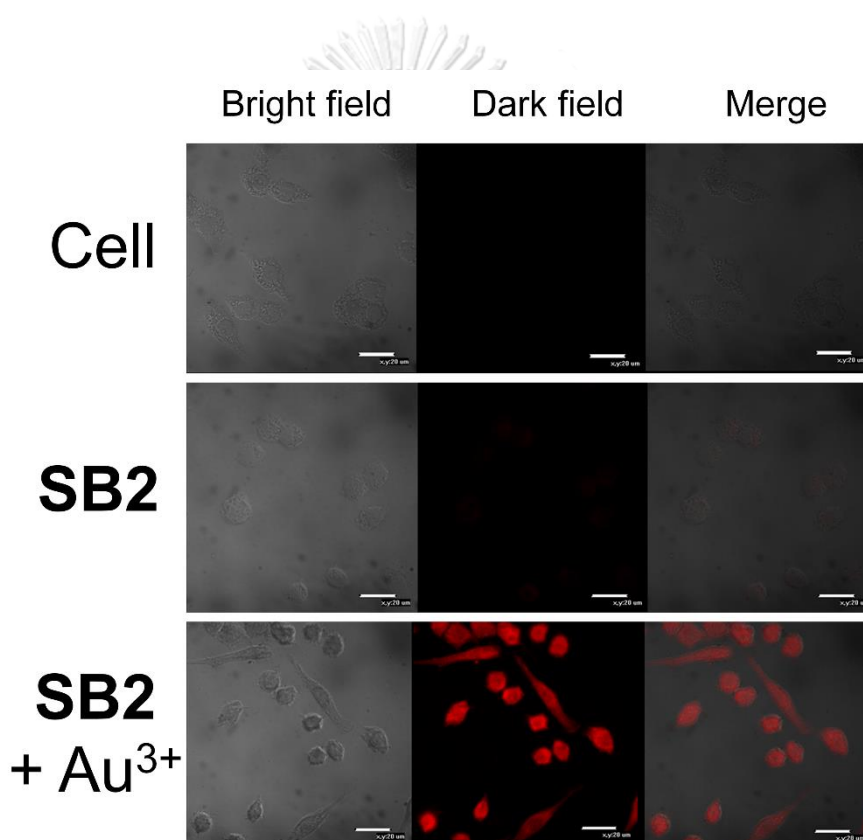
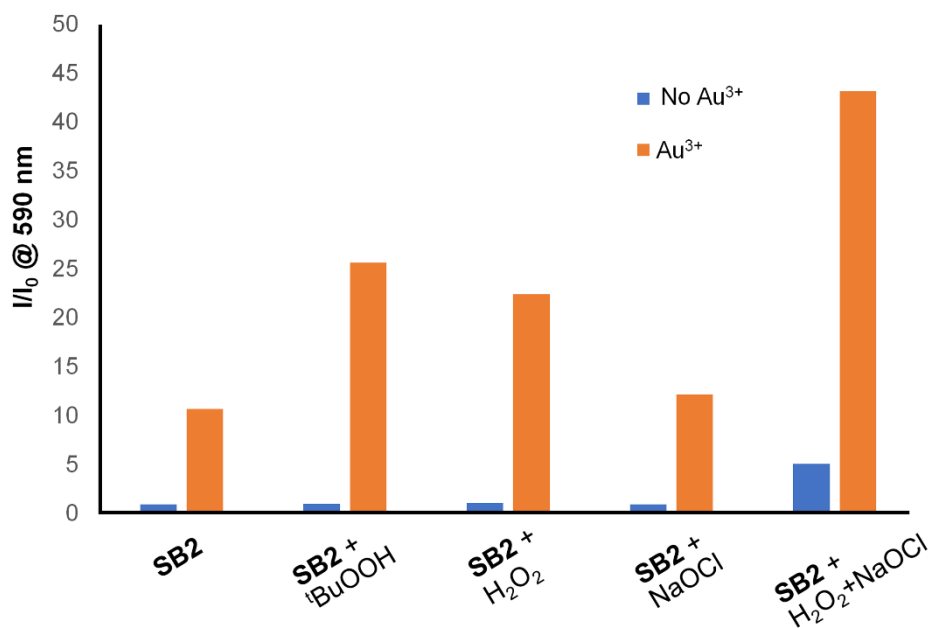


**Figure 3.35:** Confocal microscopic images ( $\lambda_{\text{Ex}}/\lambda_{\text{Em}} = 561/595 \text{ nm}$ ) of RAW264.7 macrophages before and after incubation with **SB2** ( $5 \mu\text{M}$ ), and then treated the stained cells with  $\text{Au}^{3+}$  ( $5 \mu\text{M}$ ).

### 3.4 Response of **SB2** toward ROS in the absence and presence of $\text{Au}^{3+}$

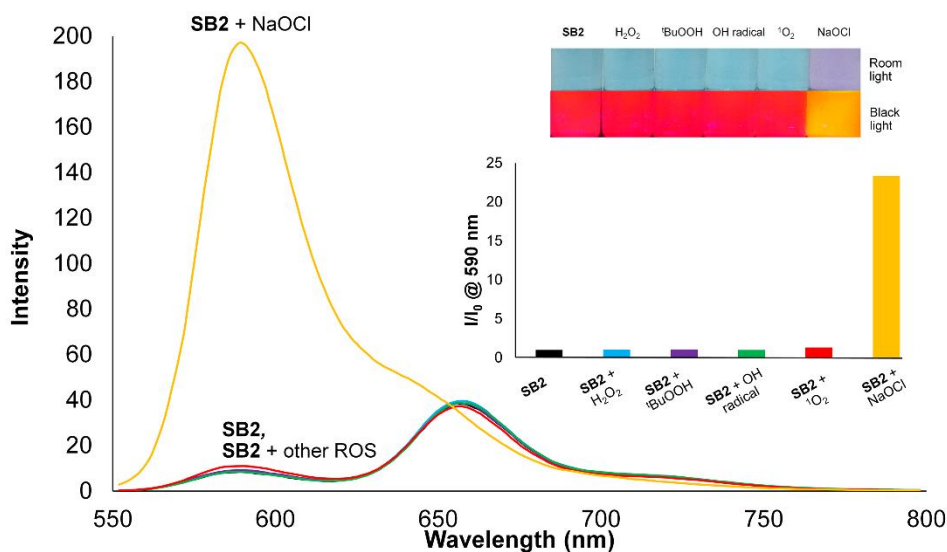
To test whether ROS could react with **SB2** catalyzed by  $\text{Au}^{3+}$ , we then monitored fluorescent change of **SB2** at 590 nm in the absence and presence of  $\text{Au}^{3+}$  (1 equivalent) toward various ROS (10 equivalents) including  $^t\text{BuOOH}$ ,  $\text{H}_2\text{O}_2$ ,  $\text{NaOCl}$  and combination of  $\text{H}_2\text{O}_2$  and

NaOCl (Figure 3.36). The result showed that **SB2** in the presence of  $\text{Au}^{3+}$  provided higher fluorescent enhancement ratio upon addition of all ROS in comparison without the addition of ROS. Surprisingly, neat **SB2** showed small response with mixture of  $\text{H}_2\text{O}_2$  and NaOCl. This result suggested that oxidation of **SB2** might not need  $\text{Au}^{3+}$  as catalyst if a certain condition was met.



**Figure 3.36:** Enhancement ratio at 590 nm ( $\lambda_{\text{ex}} = 540$  nm) of **SB2** (5  $\mu\text{M}$ ) toward various ROS (50  $\mu\text{M}$ ) with or without  $\text{Au}^{3+}$  (5  $\mu\text{M}$ ). All samples were measured after 30 minutes of mixing in solution (4/1 v/v of MeOH/HEPES buffer pH 7).

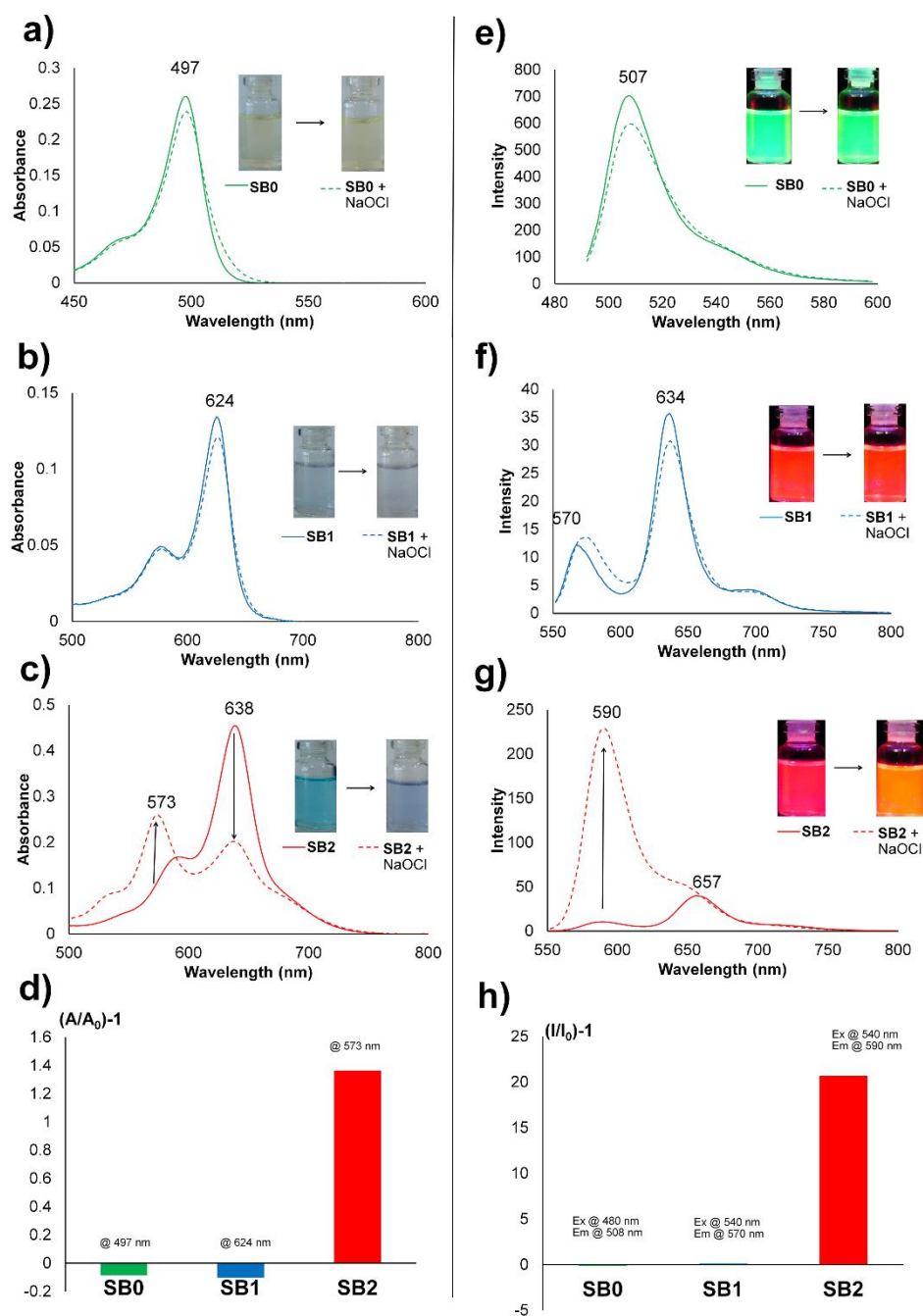
With above results, we revisited the sensing condition of **SB2**. The amount of tested ROS was reduced from 10 to 2.5 equivalents. Other new ROS were also screened, including  $^1\text{O}_2$  (generated from  $(\text{Na}_2\text{MoO}_4/\text{H}_2\text{O}_2)$ ) and  $\bullet\text{OH}$  (generated from  $(\text{NH}_4)_2\text{Fe}(\text{SO}_4)_2/\text{H}_2\text{O}_2$ ) (Figure 3.37). Both colorimetric (from blue into purple) and fluorometric responses (from red into orange) were found in case of NaOCl and 25-fold enhancement ratio was observed upon addition of 2.5 equivalents NaOCl. Therefore, **SB2** offered an opportunity as a potential fluorescent probe for NaOCl detection in biological system.



**Figure 3.37:** Emission spectra ( $\lambda_{\text{Ex}} = 540 \text{ nm}$ ) of  $5 \mu\text{M}$  **SB2** toward various ROS (2.5 equivalents), inset: enhancement ratio and Images of each solution. All samples were measured after 30 minutes of mixing in solution (3/2 v/v of MeOH/PBS (10 mM) pH 7.4).

With the above results, **SB0** and **SB1** were also tested with NaOCl and compared with **SB2** as seen in Figure 3.38. While **SB2** gave dramatic response as seen in both absorption and emission spectra (Figure 3.38c,g), there was no notable change on absorption and emission spectra of **SB0** (Figure 3.38a,e) and **SB1** (Figure 3.38b,e) upon addition of 1 equivalent NaOCl. These results suggested that both styryl group and phenolic group contained in **SB2** are necessary as receptor for NaOCl sensing.

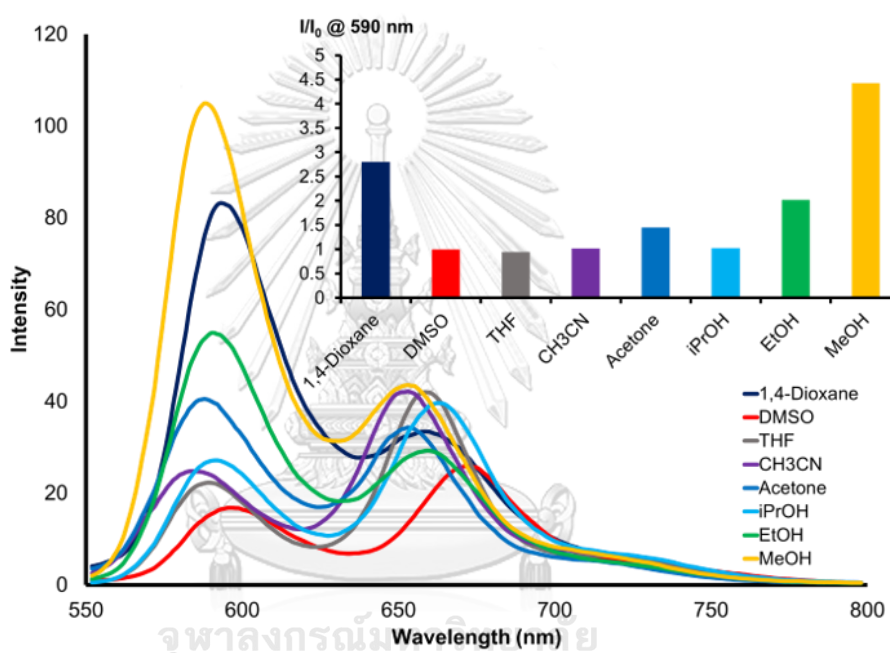




**Figure 3.38:** Absorption (a–c) and emission (e–g; excitation wavelength at 480 nm for SB0 and 540 nm for SB1 and SB2) spectra of SB0, SB1 and SB2 (5  $\mu$ M) in the absence (bold line) and presence (dash line) of 1 equivalent NaOCl. Absorbance (d) and fluorescence (h) enhancement ratio. All samples were measured after 30 minutes of mixing in 4/1 (v/v) of MeOH/PBS (10 mM) pH 7.4.

### 3.5 Optimization condition for SB2 toward NaOCl sensing

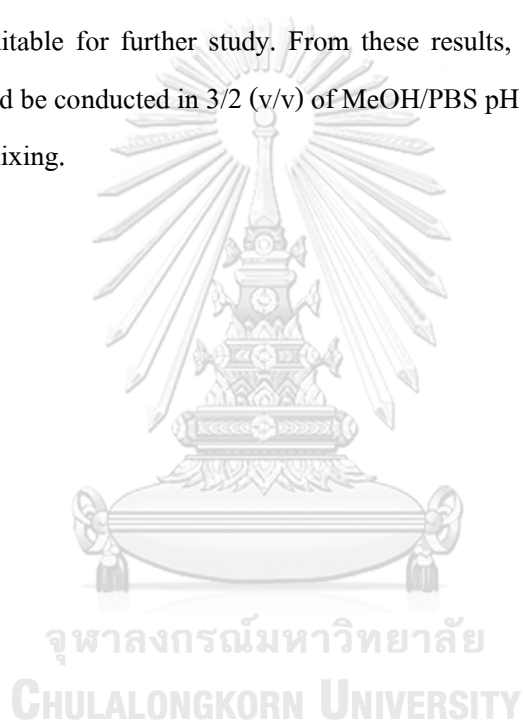
Due to poor solubility of **SB2** in pure water, organic solvent is then necessary as a co-solvent. Therefore, we varied mediums to achieve the maximum sensitivity of **SB2** toward NaOCl at 590 nm. Emission spectra of **SB2** in the presence of 1 equivalent NaOCl in various organic solvents together with enhancement ratios are shown in Figure 3.39. The result indicated that methanol still provided the highest sensitivity for NaOCl detection. Therefore, methanol was chosen as co-solvent for further study.



**Figure 3.39:** Emission spectra ( $\lambda_{\text{Ex}} = 540 \text{ nm}$ ) of  $5 \mu\text{M}$  **SB2** in various organic solvents after addition of 1 equivalent NaOCl for 30 minutes. Inset: Fluorescence enhancement ratios at 590 nm.

In the future, we plan to use our probe for intracellular detection in aqueous media. Therefore, the maximum content of water in methanol media that allows **SB2** to be operated need to be investigated. Effect of solvent ratio of methanol in water on **SB2** was evaluated as seen in Figure 3.40a. Acceptable fluorescent enhancement could be observed in range of 40–100% MeOH which reached its maximum at 80% MeOH. We decided to choose 60% MeOH (MeOH/H<sub>2</sub>O, 3/2 v/v) for further study due to its high response and high water content. Next, we studied pH effect on **SB2** using phosphate buffer saline (PBS) as a buffer and adjusted pH value

by HCl and NaOH. Fluorescent emission maxima of **SB2** alone at 590 nm (Figure 3.40b blue line) did not change under studied pH range. However, under pH range 5–10 (Figure 3.40b red line), fluorescent enhancement was observed under treatment of NaOCl. Due to pH 7.4 is a physiological pH in biological cell, so we chose such pH for further study. Lastly, we studied time profile of fluorescent enhancement ratio of **SB2** in the presence of 1 and 2.5 equivalents NaOCl (Figure 3.40c). This investigation will clarify the minimum time requirement for the sensing probe toward NaOCl. The result showed that enhancement ratio reached its saturation within 30 minutes toward both concentrations of NaOCl. So, the measurement after 30 minutes of mixing should be suitable for further study. From these results, optimal condition of **SB2** for NaOCl sensing should be conducted in 3/2 (v/v) of MeOH/PBS pH 7.4 and will be measured after 30 minutes time of mixing.



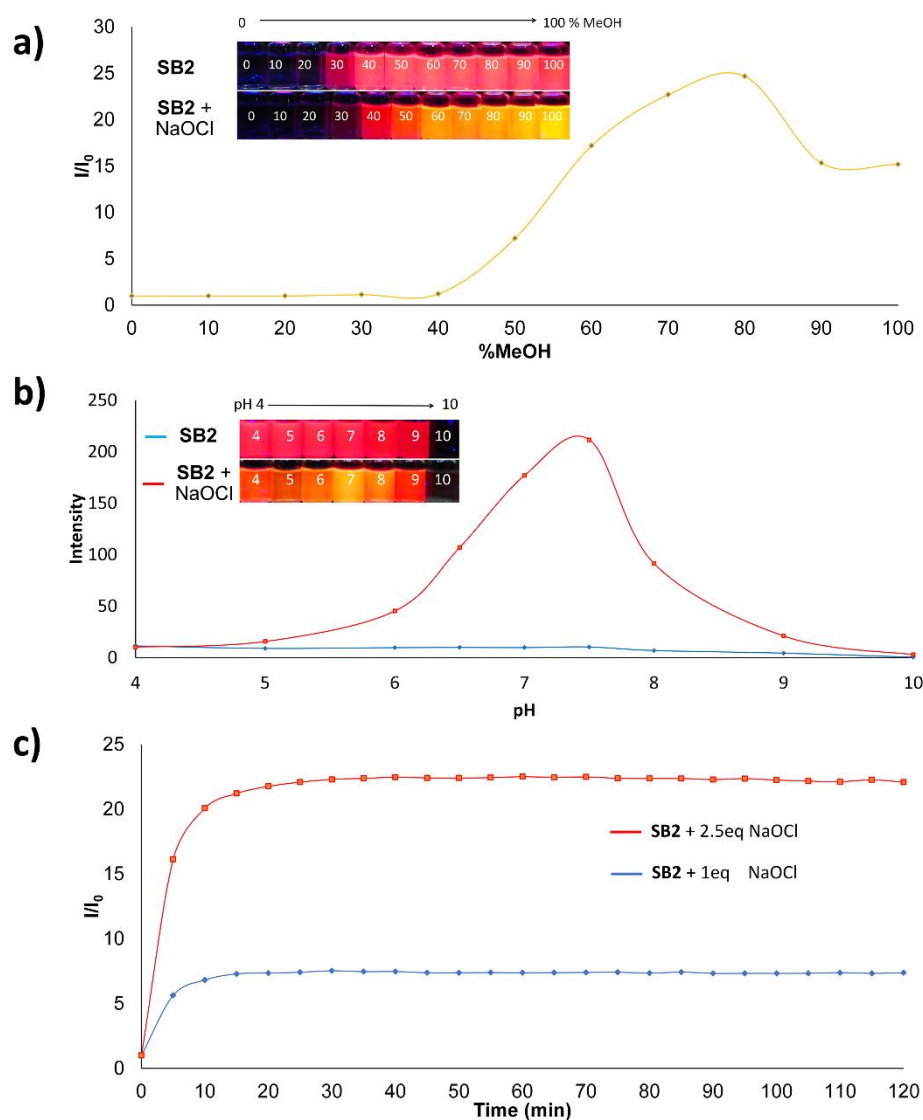


**Figure 3.40:** a) Fluorescence enhancement ratio of **SB2** in 0–100% MeOH before and after addition of 2.5 equivalents NaOCl for 30 minutes. Inset: Images of the solutions under black light in the absence and presence of NaOCl. b) Fluorescent intensity of **SB2** in 3/2 (v/v) of MeOH/PBS (10 mM) pH 4–10 in the absence and presence of 2.5 equivalents NaOCl. c) Fluorescence enhancement ratio of **SB2** in (3/2 v/v) of MeOH/PBS (10 mM) pH 7.4 in the presence of 1 or 2.5 equivalents NaOCl at various time. All samples used 5  $\mu$ M **SB2** (excitation wavelength at 540 nm and emission wavelength at 590 nm).

### 3.6 Sensitivity of SB2 toward NaOCl

To evaluate working concentration range of NaOCl sensed by **SB2**, UV-vis and fluorescence titration spectra were performed (Figure 3.41). Upon addition of NaOCl up to 2.5

equivalents, the reduction of the absorption band at 638 nm was observed together with enhancement of an absorption band at 573 nm. Further addition of NaOCl resulted in reduction of absorption band at 573 nm along with a rise of new absorption band at 505 nm (Figure 3.41a). The solution under room light also showed the corresponding result. Two-step colorimetric transformation was observed during the titration from blue to purple at low NaOCl concentration and purple to colourless at high NaOCl concentration (Figure 3.41a inset). This result suggested that **SB2** could react with NaOCl to afford two or more intermediates with distinct absorption properties. The possible mechanism occurred between **SB2** and NaOCl will be discussed in the next section. Due to small Stokes shifts of **SB2** (19 nm, Table 3.1), absorption and emission bands are overlapped. To avoid that, 480 and 540 nm which were shorter than maximum absorption wavelengths (513 and 573 nm, respectively) were selected as two excitation wavelengths for fluorescence titration experiment. Upon excitation at 540 nm, the fluorescent intensity of **SB2** at 590 nm gradually rose toward the addition of NaOCl from 0 to 2.5 equivalents. Further addition of NaOCl up to 10 equivalents caused reduction of the intensity at 590 nm (Figure 3.41b). Upon excitation at 480 nm, similar result was observed in range of 0–2.5 equivalents of NaOCl. However, further addition of NaOCl up to 10 equivalents caused the drop of the intensity centered at 590 nm together with the rise of new peak at 513 nm (Figure 3.41c). Changes of emission intensity at the two peaks are plotted in Figure 3.41d. The solution under black light also showed the corresponding result by two-step fluorescent color change from red to orange at low NaOCl concentration and from orange to green at high NaOCl concentration (Figure 3.41d inset). Although both orange and green phase could be used to monitor NaOCl concentration, orange phase ( $\lambda_{\text{Ex}}/\lambda_{\text{Em}} = 540/590$  nm) was within our interest due to higher sensitivity for NaOCl detection. Orange phase also has an advantage of long-wavelength fluorescence in live cell application. Limit of detection (LOD) was estimated from linear relation between NaOCl concentration (0–5  $\mu\text{M}$ ) and fluorescence intensity (Figure 3.42) to be 0.26  $\mu\text{M}$ .

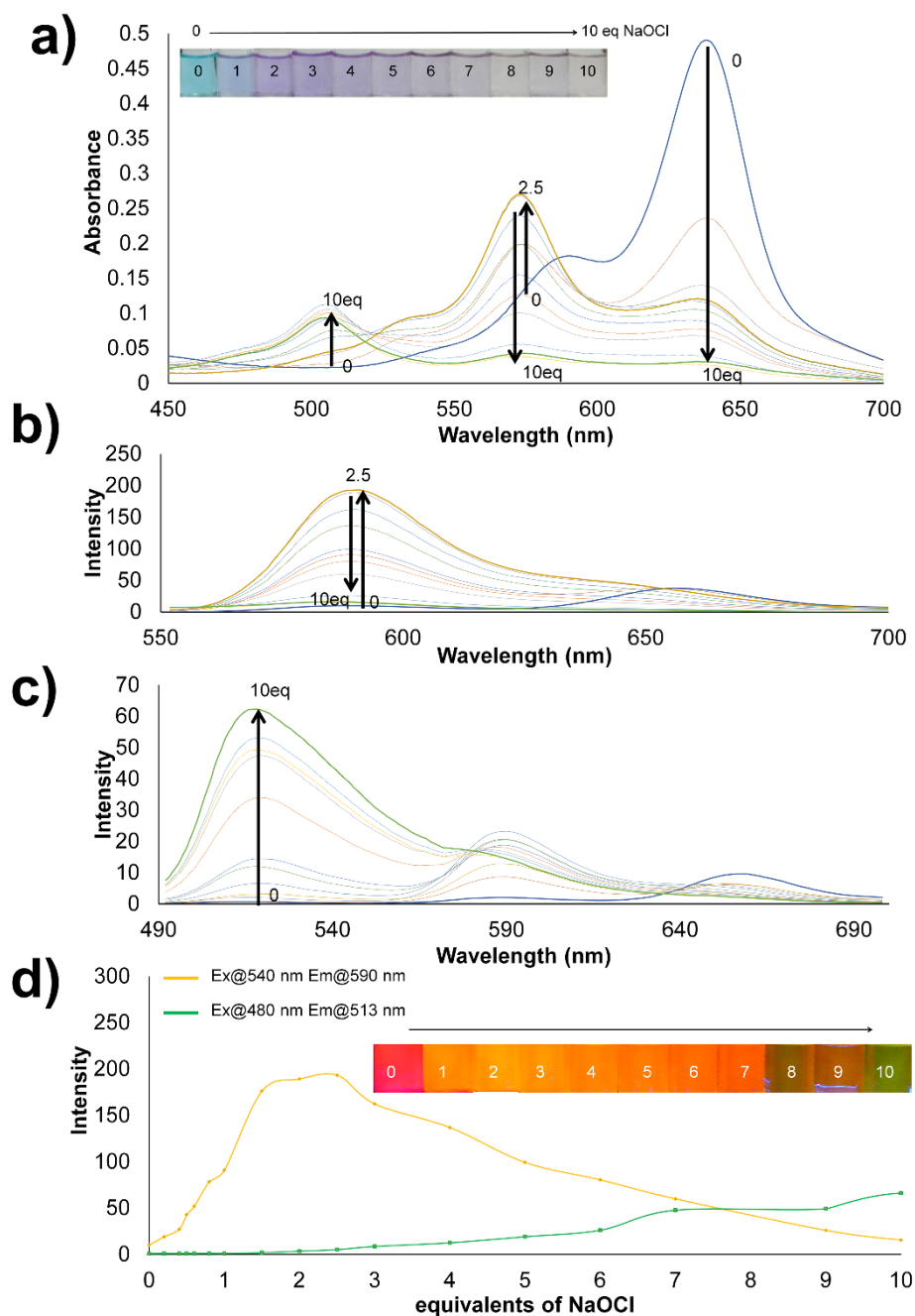


**Figure 3.41:** Absorption spectra (a), emission spectra under excitation at 540 (b) and 480 (c) nm and sensitivity plot (d) of **SB2** (5 μM) toward NaOCl (0–10 equivalents), inset: images of solutions under room light (a) and black light (d). All samples were measured after 30 minutes of mixing in 3/2 (v/v) of MeOH/PBS (10 mM) pH 7.4.

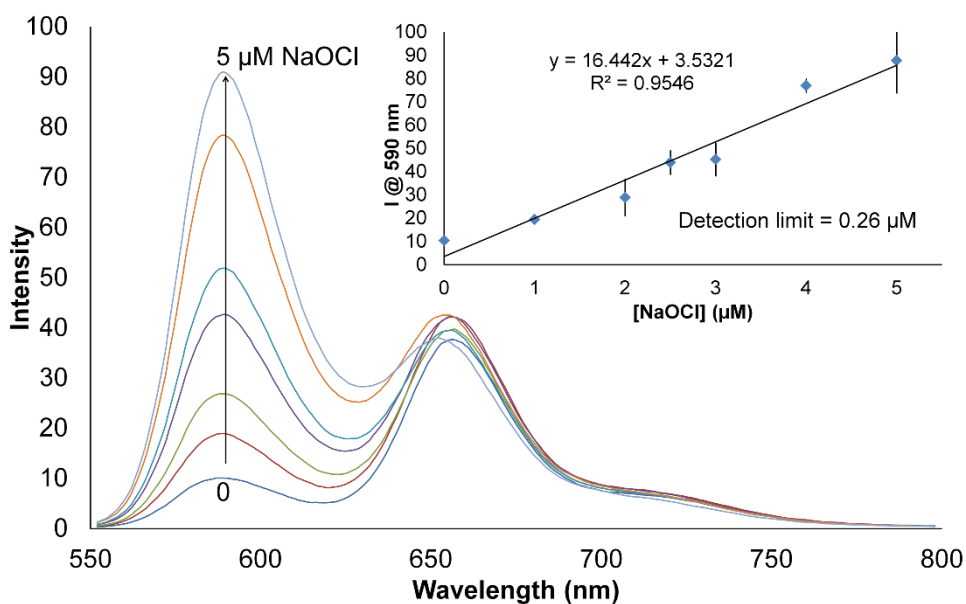


**Figure 3.42:** Emission spectra of **SB2** (5  $\mu\text{M}$ ) toward NaOCl (0–5  $\mu\text{M}$ ), inset: linear relation of fluorescence intensity vs NaOCl concentration. All samples were measured after 30 minutes of mixing in 3/2 (v/v) of MeOH/PBS (10 mM) pH 7.4.

### 3.7 Proposed reaction mechanism between **SB2** and NaOCl

To propose reaction mechanism between **SB2** and NaOCl, MALDI-TOF mass spectrometer was used to detect the intermediates and products from mixture of **SB2** (5  $\mu\text{M}$ ) and NaOCl (5 equivalents) in MeOH after 30 minutes of reaction. The mass spectrum was obtained as shown in Figure 3.43a and reaction mechanism is proposed in Figure 3.43b. A peak signal at  $m/z = 546.25$  corresponded to parent ion  $[\text{SB2}]^+$ . One double bond of **SB2** could undergo epoxidation with NaOCl followed by ring-opening hydrolysis to generate diol compound **SB2a** which was responsible for the peak signal at  $m/z = 580.30$ . Oxidation of diol moiety on **SB2a** into  $\beta$ -hydroxy ketone **SB2b** provided the peak at  $m/z = 622.16$ . These intermediates **SB2a** and **SB2b** should be responsible for the orange emission of probe **SB2** in the presence of low concentration NaOCl (< 2.5 equivalents). In the presence of high concentration NaOCl (> 2.5 equivalents), another double bond could be epoxidized to afford green-emissive products **SB2c** and **SB2d** which attributed to  $m/z$  peak at 656.29 and 640.42, respectively. Moreover, this proposed mechanism can explain how **SB2** was more reactive than **SB1** (Figure 3.38). The oxidation of the double bond in the **SB**

probe can be promoted by the strong electron-donating group, which hydroxyl group of **SB2** is stronger than methyl group of **SB1**.

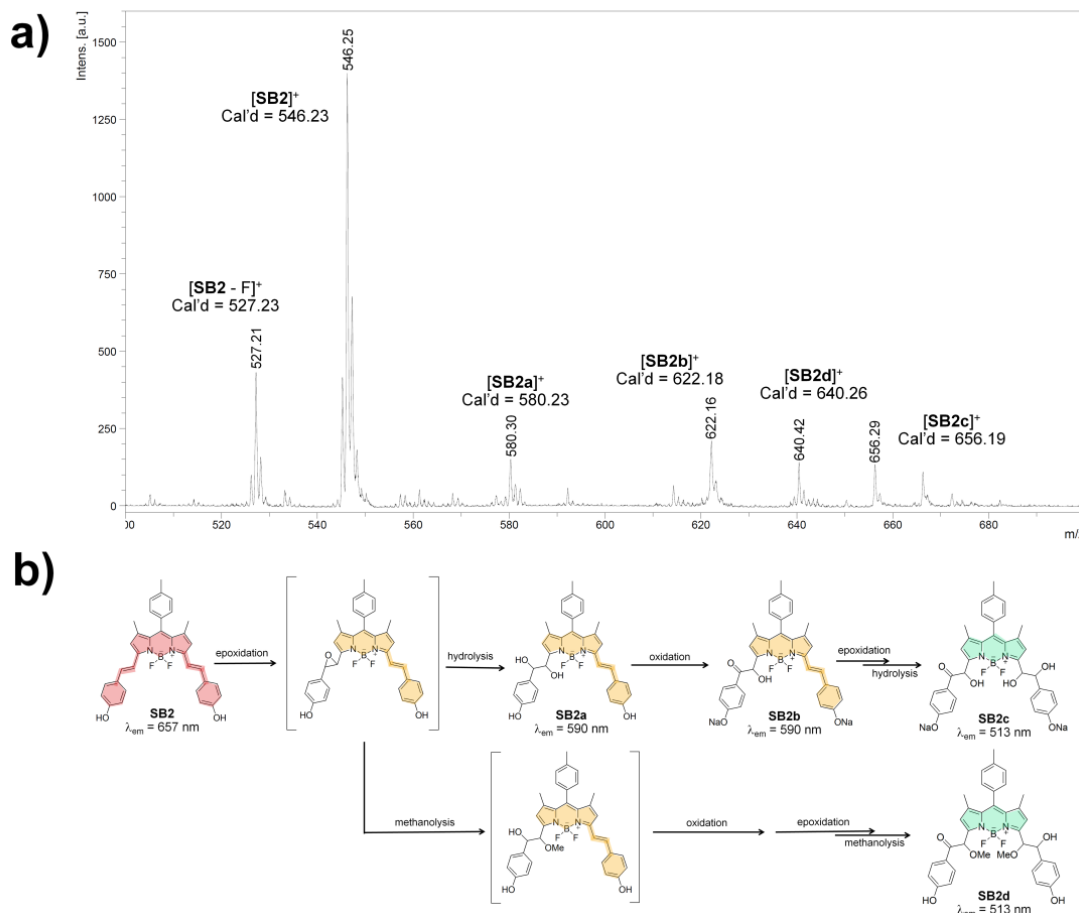


**Figure 3.43:** a) MALDI-TOF mass spectrum from mixture of **SB2** (5  $\mu\text{M}$ ) and  $\text{NaOCl}$  (5 equivalents) in  $\text{MeOH}$  and b) proposed reaction mechanism between **SB2** and  $\text{NaOCl}$ .

### 3.8 Cell-imaging application

To apply **SB2** for detection of hypochlorite in live cell imaging, we firstly determined the working concentration range without cellular cytotoxicity. We used MTT assay against RAW264.7 cells in the presence of **SB2** (1 or 10  $\mu\text{M}$ ) with or without an oxidative stress inducer, lipopolysaccharide (LPS) (Figure 3.44). The result showed that cell viability didn't significantly change from control sample, suggesting that **SB2** at concentration range from 1 to 10  $\mu\text{M}$  was not toxic to the tested cells in both normal state and stress state.



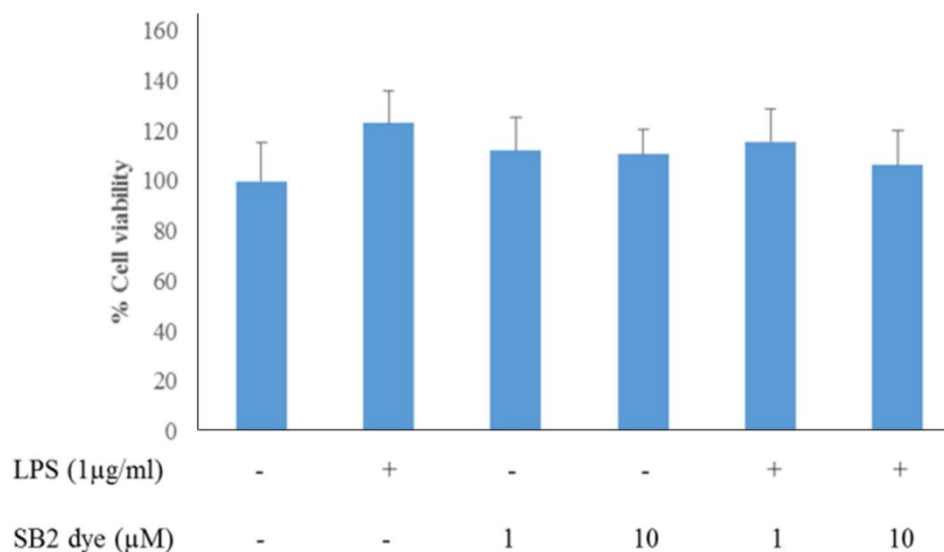


**Figure 3.44:** MTT assay against RAW264.7 cells in the absence and presence of LPS (1 µg/mL) before and after treatment with of **SB2** (1 and 10 µM).

To study the detection of ROS in live cells, the cells were induced into stress state by exogenously addition of NaOCl or endogenously generation of ROS via LPS. Fluorescence signal was recorded by confocal laser microscope ( $\lambda_{\text{ex}} = 559 \text{ nm}$ ,  $\lambda_{\text{em}} = 570\text{--}612 \text{ nm}$ ). The result showed that there was no fluorescent signal observed in the cells both in the absence and presence of **SB2** (1 µM, Figure 3.45a and b) because biomolecules in the cells and the probe **SB2** did not emit fluorescence in the monitoring range. When the **SB2**-stained cells were treated with 1 µM NaOCl, fluorescent signal was observed in the cytoplasm (Figure 3.45c). This result proved that exogenous NaOCl penetrated cell membrane and transformed **SB2** in cytoplasm into orange-emissive product which could be detected in the monitoring range. The orange fluorescent signal became weaker upon addition of high concentration NaOCl (> 2.5 µM, Figure 3.45d and e). This result agreed with the proposed mechanism discussed earlier (Figure 3.43b).

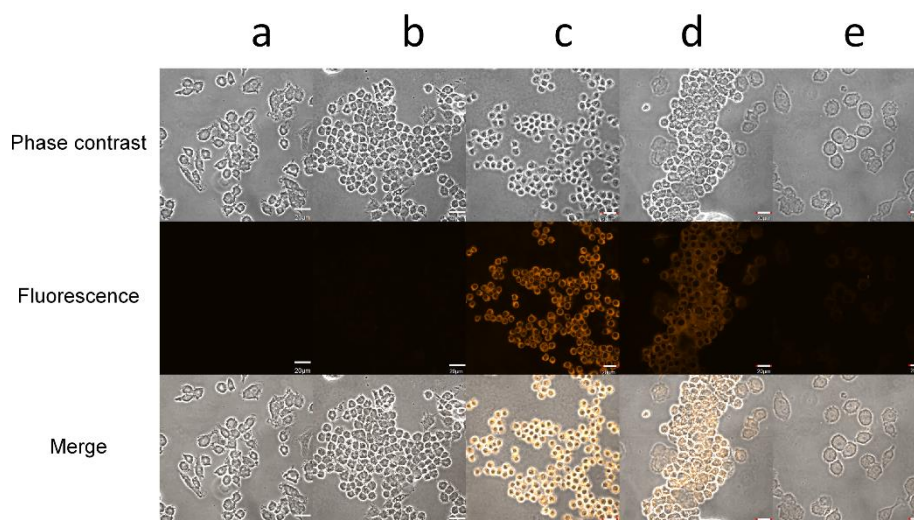


**Figure 3.45:** Confocal microscopic images of murine macrophages RAW264.7 before (a) and after (b) incubation with **SB2** (1  $\mu\text{M}$ ) followed by treatment with NaOCl at 1 (c), 2.5 (d) or 10  $\mu\text{M}$  (e).

In case of endogenous ROS, LPS was introduced in the culture medium at various concentration (0–10  $\mu\text{g}/\text{mL}$ ) to stimulate the cells before the incubation with **SB2** (1  $\mu\text{M}$ ). Orange fluorescent intensity was enhanced along with the concentration of LPS (Figure 3.46). This result suggested that the probe **SB2** could response to the endogenously generated HOCl/CIO<sup>-</sup>. However, mean grey value estimated by ImageJ program (Figure 3.47) clearly showed that the fluorescent intensity reached its maximum at 2.5  $\mu\text{g}/\text{mL}$  LPS and remained steady up to 10  $\mu\text{g}/\text{mL}$  LPS, which is different from exogenous NaOCl result. We hypothesized that living cell may have a metabolism to limit the generation of endogenous HOCl/CIO<sup>-</sup> stimulated by LPS. Another hypothesis is that the probes might be oxidized by other ROS which was also generated from LPS along with HOCl/CIO<sup>-</sup> through a different mechanism. Nevertheless, **SB2** is still potentially useful for detection of endogenous ROS induced by a wide concentration range of LPS.

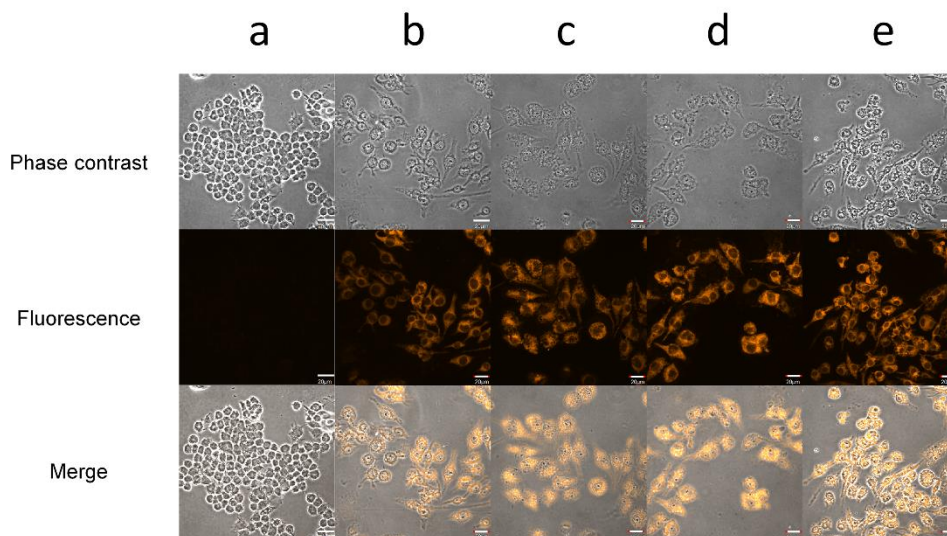


**Figure 3.46:** Confocal microscopic images of murine macrophages RAW264.7 in the absence (a) and presence of LPS at 0.1 (b), 1 (c), 2.5 (d) and 10  $\mu\text{g/mL}$  (e) after incubation with SB2 (1  $\mu\text{M}$ ).

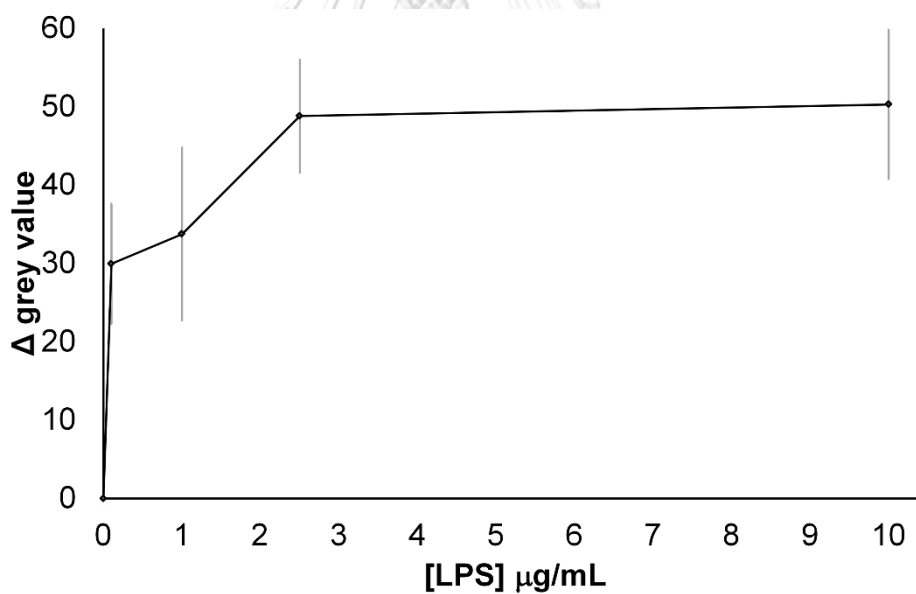
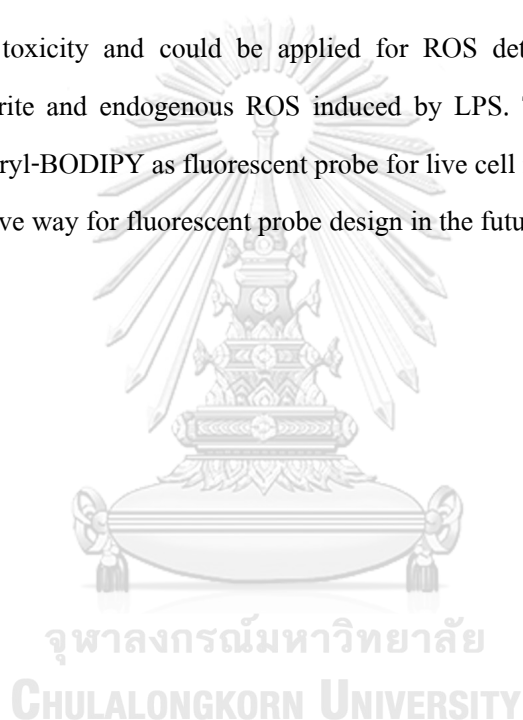


**Figure 3.47:** Mean grey values (subtracted by blank) of fluorescent signal from SB2 in RAW264.7 cells stimulated with LPS at 0–10  $\mu\text{g/mL}$ .

## CHAPTER IV CONCLUSIONS

In summary, a new orange-emissive fluorescent probe based on BODIPY **SB2** has been developed for detection of ROS. The attachment of 4-vinylphenol groups to BODIPY core provides red emission wavelength due to the  $\pi$ -conjugated extension together with reactive double bond as a receptor for oxidation reaction. The probe was selective to NaOCl over other ROS, resulted in colorimetric change from blue to purple and turn-on orange fluorescent intensity (up to 25-fold). Limit of detection toward NaOCl was estimated to be 0.26  $\mu\text{M}$ . Moreover, **SB2** showed no cellular toxicity and could be applied for ROS detection in live cells for both exogenous hypochlorite and endogenous ROS induced by LPS. The outcome of this research renders the use of styryl-BODIPY as fluorescent probe for live cell imaging of HOCl/CIO<sup>-</sup> and offers a new alternative way for fluorescent probe design in the future.





จุฬาลงกรณ์มหาวิทยาลัย  
**CHULALONGKORN UNIVERSITY**

## REFERENCES

1. Finkel, T., Oxidant signals and oxidative stress. *Current Opinion in Cell Biology* **2003**, *15* (2), 247-254.
2. Pullar, J. M.; Vissers, M. C. M.; Winterbourn, C. C., Living with a Killer: The Effects of Hypochlorous Acid on Mammalian Cells. *IUBMB Life* **2000**, *50* (4 - 5), 259-266.
3. Steinbeck, M. J.; Nesti, L. J.; Sharkey, P. F.; Parvizi, J., Myeloperoxidase and Chlorinated Peptides in Osteoarthritis: Potential Biomarkers of the Disease. *Journal of orthopaedic research : official publication of the Orthopaedic Research Society* **2007**, *25* (9), 1128-1135.
4. Sugiyama, S.; Okada, Y.; Sukhova, G. K.; Virmani, R.; Heinecke, J. W.; Libby, P., Macrophage Myeloperoxidase Regulation by Granulocyte Macrophage Colony-Stimulating Factor in Human Atherosclerosis and Implications in Acute Coronary Syndromes. *The American Journal of Pathology* **2001**, *158* (3), 879-891.
5. Yap, Y. W.; Whiteman, M.; Cheung, N. S., Chlorinative stress: An under appreciated mediator of neurodegeneration? *Cellular Signalling* **2007**, *19* (2), 219-228.
6. Malle, E.; Buch, T.; Grone, H.-J., Myeloperoxidase in kidney disease. *Kidney International* **2003**, *64* (6), 1956-1967.
7. Batandier, C.; Fontaine, E.; Kériel, C.; Leverve, X. M., Determination of mitochondrial reactive oxygen species: methodological aspects. *Journal of Cellular and Molecular Medicine* **2002**, *6* (2), 175-187.
8. Fernández-Castro, P.; Vallejo, M.; San Román, M. F.; Ortiz, I., Insight on the fundamentals of advanced oxidation processes. Role and review of the determination methods of reactive oxygen species. *Journal of Chemical Technology & Biotechnology* **2015**, *90* (5), 796-820.
9. Chan, J.; Dodani, S. C.; Chang, C. J., Reaction-based small-molecule fluorescent probes for chemoselective bioimaging. *Nature Chemistry* **2012**, *4*, 973.
10. Chen, X.; Tian, X.; Shin, I.; Yoon, J., Fluorescent and luminescent probes for detection of reactive oxygen and nitrogen species. *Chemical Society Reviews* **2011**, *40* (9), 4783-4804.
11. Maulucci, G.; Bačić, G.; Bridal, L.; Schmidt, H. H. H. W.; Tavitian, B.; Viel, T.; Utsumi, H.; Yalçın, A. S.; De Spirito, M., Imaging Reactive Oxygen Species-Induced

Modifications in Living Systems. *Antioxidants & Redox Signaling* **2016**, *24* (16), 939-958.

12. Wang, H.-S., Development of fluorescent and luminescent probes for reactive oxygen species. *TrAC Trends in Analytical Chemistry* **2016**, *85*, 181-202.

13. Pak, Y. L.; Park, S. J.; Wu, D.; Cheon, B.; Kim, H. M.; Bouffard, J.; Yoon, J., N-Heterocyclic Carbene Boranes as Reactive Oxygen Species-Responsive Materials: Application to the Two-Photon Imaging of Hypochlorous Acid in Living Cells and Tissues. *Angewandte Chemie International Edition* **2018**, *57* (6), 1567-1571.

14. Jun, Y. W.; Sarkar, S.; Singha, S.; Reo, Y. J.; Kim, H. R.; Kim, J.-J.; Chang, Y.-T.; Ahn, K. H., A two-photon fluorescent probe for ratiometric imaging of endogenous hypochlorous acid in live cells and tissues. *Chemical Communications* **2017**, *53* (78), 10800-10803.

15. Chang, M. C. Y.; Pralle, A.; Isacoff, E. Y.; Chang, C. J., A Selective, Cell-Permeable Optical Probe for Hydrogen Peroxide in Living Cells. *Journal of the American Chemical Society* **2004**, *126* (47), 15392-15393.

16. Kim, M.; Ko, S.-K.; Kim, H.; Shin, I.; Tae, J., Rhodamine cyclic hydrazide as a fluorescent probe for the detection of hydroxyl radicals. *Chemical Communications* **2013**, *49* (72), 7959-7961.

17. Meng, L.; Wu, Y.; Yi, T., A ratiometric fluorescent probe for the detection of hydroxyl radicals in living cells. *Chemical Communications* **2014**, *50* (37), 4843-4845.

18. Loudet, A.; Burgess, K., BODIPY Dyes and Their Derivatives: Syntheses and Spectroscopic Properties. *Chemical Reviews* **2007**, *107* (11), 4891-4932.

19. Deng, X.; Min, B. K.; Guloy, A.; Friend, C. M., Enhancement of O<sub>2</sub> Dissociation on Au(111) by Adsorbed Oxygen: Implications for Oxidation Catalysis. *Journal of the American Chemical Society* **2005**, *127* (25), 9267-9270.

20. Gualandi, I.; Tonelli, D., A new electrochemical sensor for OH radicals detection. *Talanta* **2013**, *115*, 779-786.

21. Rosen, G. M.; Tsai, P.; Barth, E. D.; Dorey, G.; Casara, P.; Spedding, M.; Halpern, H. J., A One-Step Synthesis of 2-(2-Pyridyl)-3H-indol-3-one N-Oxide: Is It an Efficient Spin Trap for Hydroxyl Radical? *The Journal of Organic Chemistry* **2000**, *65* (14), 4460-4463.

22. Nobushi, Y.; Uchikura, K., Selective Detection of Hydroxyl Radical Scavenging Capacity Based on Electrogenenerated Chemiluminescence Detection Using Tris(2,2'-

- bipyridine)ruthenium(III) by Flow Injection Analysis. *Chemical and Pharmaceutical Bulletin* **2010**, 58 (1), 117-120.
23. Xu, X.; Duan, X.; Yi, Z.; Zhou, Z.; Fan, X.; Wang, Y., Photocatalytic production of superoxide ion in the aqueous suspensions of two kinds of ZnO under simulated solar light. *Catalysis Communications* **2010**, 12 (3), 169-172.
24. Lichtman, J. W.; Conchello, J.-A., Fluorescence microscopy. *Nature Methods* **2005**, 2 (12), 910-919.
25. Sukato, R.; Sangpetch, N.; Palaga, T.; Jantra, S.; Vchirawongkwin, V.; Jongwohan, C.; Sukwattanasinitt, M.; Wacharasindhu, S., New turn-on fluorescent and colorimetric probe for cyanide detection based on BODIPY-salicylaldehyde and its application in cell imaging. *Journal of Hazardous Materials* **2016**, 314, 277-285.
26. Liu, M.; Yu, X.; Li, M.; Liao, N.; Bi, A.; Jiang, Y.; Liu, S.; Gong, Z.; Zeng, W., *Fluorescent probes for the detection of magnesium ions (Mg<sup>2+</sup>): From design to application*. 2018; Vol. 8, p 12573-12587.
27. Zhang, W.; Ma, Z.; Du, L.; Li, M., Design strategy for photoinduced electron transfer-based small-molecule fluorescent probes of biomacromolecules. *Analyst* **2014**, 139 (11), 2641-2649.
28. Chen, K.-Y.; Tsai, H.-Y., *Synthesis, X-ray Structure, Spectroscopic Properties and DFT Studies of a Novel Schiff Base*. 2014; Vol. 15, p 18706-18724.
29. Shrestha, D.; Jenei, A.; Nagy, P.; Vereb, G.; Szollosi, J., *Understanding FRET as a Research Tool for Cellular Studies*. 2015; Vol. 16, p 6718-6756.
30. Long, L.; Zhang, D.; Li, X.; Zhang, J.; Zhang, C.; Zhou, L., A fluorescence ratiometric sensor for hypochlorite based on a novel dual-fluorophore response approach. *Analytica Chimica Acta* **2013**, 775, 100-105.
31. He, Y.; Miao, L.; Yu, L.; Chen, Q.; Qiao, Y.; Zhang, J.-F.; Zhou, Y., A near-infrared fluorescent probe for detection of exogenous and endogenous hydrogen peroxide in vivo. *Dyes and Pigments* **2019**, 168, 160-165.
32. Kim, T.-I.; Park, S.; Choi, Y.; Kim, Y., A BODIPY-Based Probe for the Selective Detection of Hypochlorous Acid in Living Cells. *Chemistry – An Asian Journal* **2011**, 6 (6), 1358-1361.
33. Lei, K.; Sun, M.; Du, L.; Zhang, X.; Yu, H.; Wang, S.; Hayat, T.; Alsaedi, A., Sensitive



determination of endogenous hydroxyl radical in live cell by a BODIPY based fluorescent probe.

*Talanta* **2017**, *170*, 314-321.

34. Xu, X.-x.; Qian, Y., A novel pyridyl triphenylamine–BODIPY aldoxime: Naked-eye visible and fluorometric chemodosimeter for hypochlorite. *Spectrochimica Acta Part A: Molecular and Biomolecular Spectroscopy* **2017**, *183*, 356-361.

35. Xu, C.; Qian, Y., A selenamorpholine-based redox-responsive fluorescent probe for targeting lysosome and visualizing exogenous/endogenous hydrogen peroxide in living cells and zebrafish. *Journal of Materials Chemistry B* **2019**, *7* (16), 2714-2721.

36. Li, Z.; Brouwer, C.; He, C., Gold-Catalyzed Organic Transformations. *Chemical Reviews* **2008**, *108* (8), 3239-3265.

37. Barluenga, J.; Diéguez, A.; Fernández, A.; Rodríguez, F.; Fañanás, F. J., Gold- or Platinum-Catalyzed Tandem Cycloisomerization/Prins-Type Cyclization Reactions. *Angewandte Chemie International Edition* **2006**, *45* (13), 2091-2093.

38. Rozenman, M. M.; Kanan, M. W.; Liu, D. R., Development and Initial Application of a Hybridization-Independent, DNA-Encoded Reaction Discovery System Compatible with Organic Solvents. *Journal of the American Chemical Society* **2007**, *129* (48), 14933-14938.

39. Corma, A.; Serna, P., Preparation of substituted anilines from nitro compounds by using supported gold catalysts. *Nature Protocols* **2006**, *1* (6), 2590-2595.

40. Boehme, K.; Brauer, H. D., Generation of singlet oxygen from hydrogen peroxide disproportionation catalyzed by molybdate ions. *Inorganic Chemistry* **1992**, *31* (16), 3468-3471.

41. Zheng, Y.; Zhang, X.; Yao, Y.; Chen, X.; Yang, Q., Ultra-small Au nanoparticles stabilized by silica hollow nanospheres for styrene oxidation with oxygen. *RSC Advances* **2015**, *5* (128), 105747-105752.

## APPENDIX

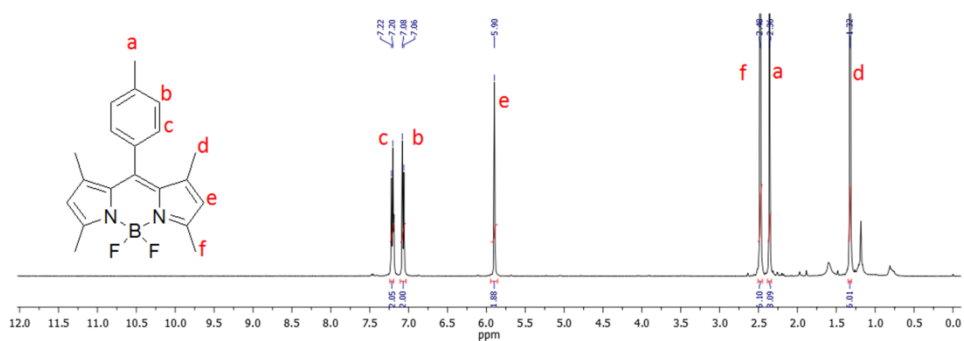


Figure A.48: <sup>1</sup>H-NMR spectrum of SB0 in CDCl<sub>3</sub>

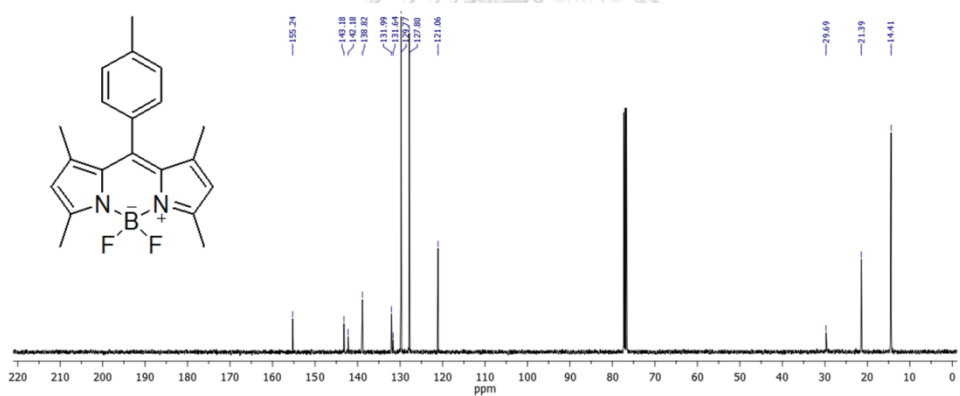


Figure A.49: <sup>13</sup>C-NMR spectrum of SB0 in CDCl<sub>3</sub>

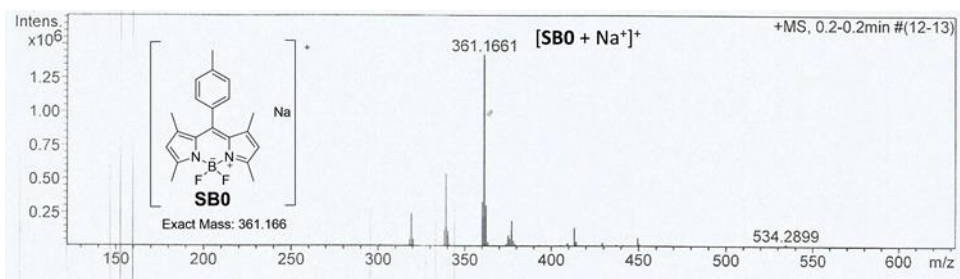


Figure A.50: ESI-HRMS spectrum of SB0

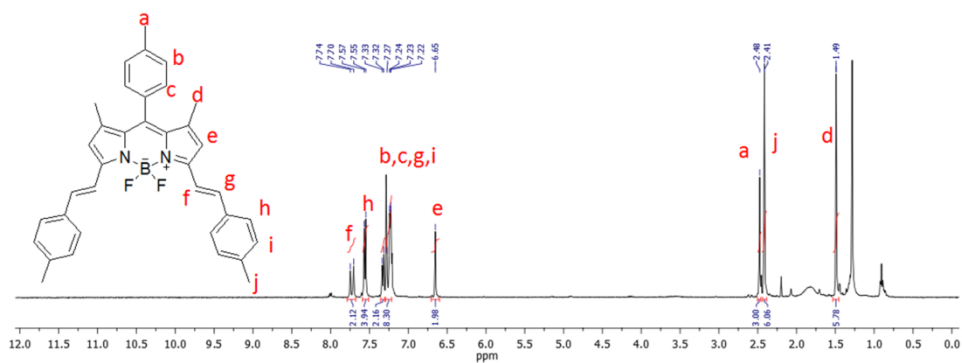


Figure A.51:  $^1\text{H}$ -NMR spectrum of SB1 in  $\text{CDCl}_3$

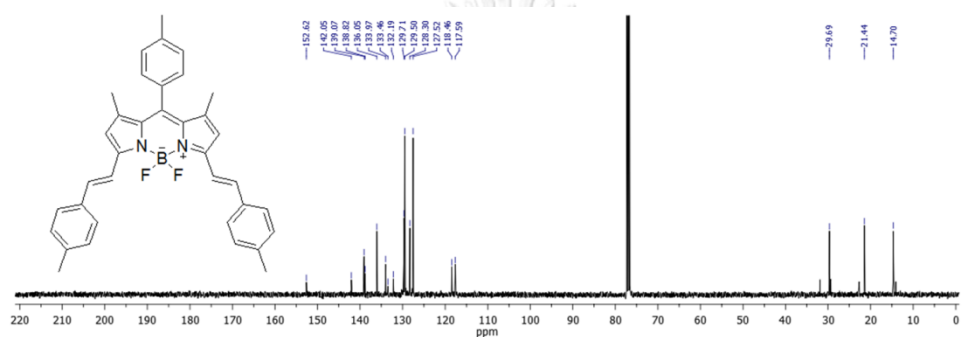


Figure A.52:  $^{13}\text{C}$ -NMR spectrum of SB1 in  $\text{CDCl}_3$

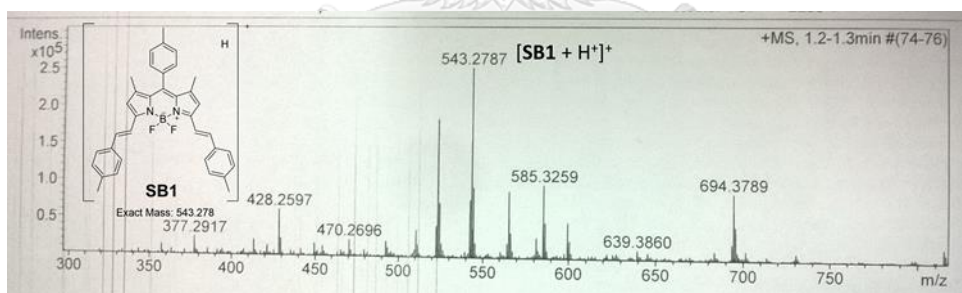


Figure A.53: ESI-HRMS spectrum of SB1

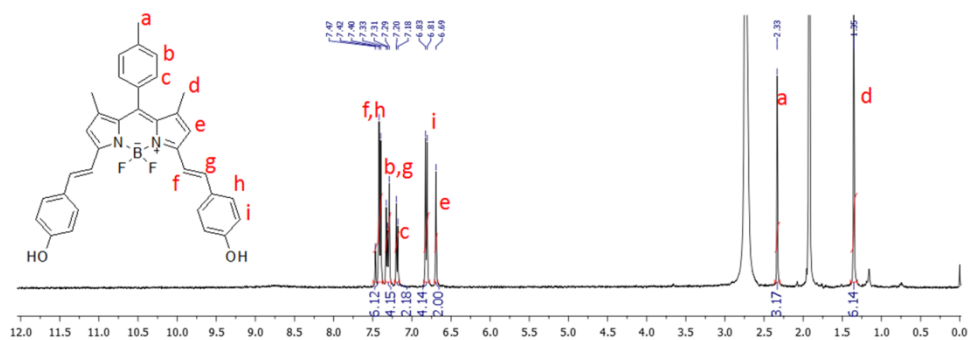


Figure A.54:  $^1\text{H}$ -NMR spectrum of SB2 in acetone- $\text{D}_6$

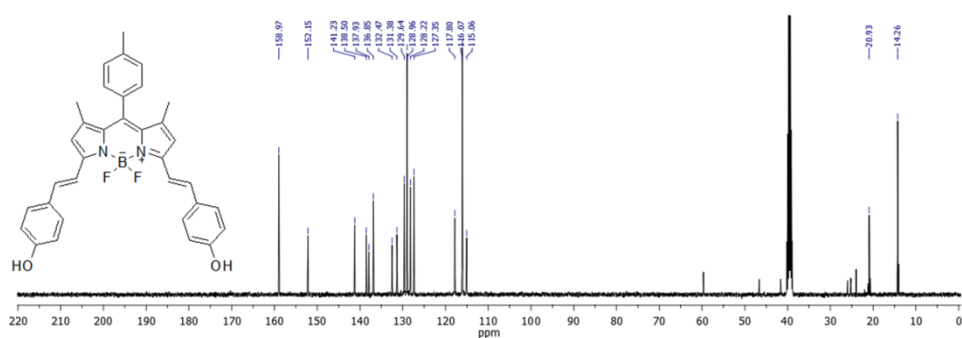


Figure A.55:  $^{13}\text{C}$ -NMR spectrum of SB2 in DMSO- $\text{D}_6$

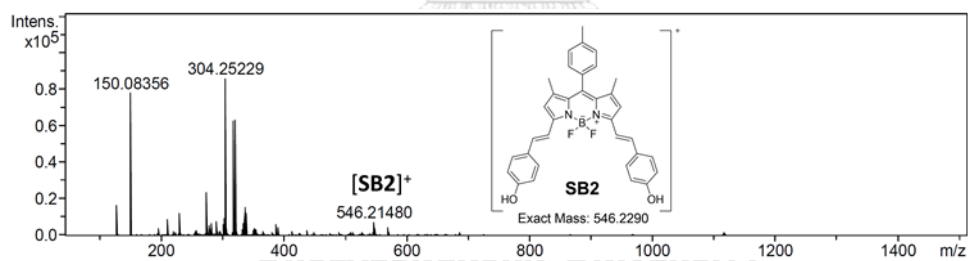


Figure A.56: ESI-HRMS spectrum of SB2





จุฬาลงกรณ์มหาวิทยาลัย  
**CHULALONGKORN UNIVERSITY**

## VITA

**NAME** Suthikorn Jantra

**DATE OF BIRTH** 30 September 1990

**PLACE OF BIRTH** Bangkok, Thailand

**INSTITUTIONS ATTENDED** Chulalongkorn University

**HOME ADDRESS** 8/29 Sirinakorn Village, Soi Phaholyothin 54/1 Yak 1,  
Leabklongsong Road, Kwang Saimai, Saimai District, Bangkok  
10220

**PUBLICATION**

1. Journal of Hazardous Materials 2016, 314, 277–285.
2. Dyes and Pigments 2019, 162, 189–195.